

# Communication-and-Energy Efficient Over-the-Air Federated Learning

Yipeng Liang<sup>ID</sup>, Graduate Student Member, IEEE, Qimei Chen<sup>ID</sup>, Member, IEEE, Guangxu Zhu<sup>ID</sup>, Member, IEEE, Hao Jiang<sup>ID</sup>, Member, IEEE, Yonina C. Eldar<sup>ID</sup>, Fellow, IEEE, and Shuguang Cui<sup>ID</sup>, Fellow, IEEE

**Abstract**—Communication and energy efficiencies are two crucial objectives in the pursuit of edge intelligence in 6G networks, and become increasingly important given the prevalence of large model training. Existing designs typically focus on either communication efficiency or energy efficiency due to the fact that improving one objective generally comes at the expense of the other. *Over-the-air federated learning (OTA-FL)* has recently emerged as a promising approach to enhance both efficiencies through an integrated communication and computation design. Nevertheless, most previous studies on OTA-FL only consider scenarios where the dataset for the entire FL procedure is collected and available prior to training. In real-world applications, devices continuously collect new data in an online manner. This underscores the significance of sample collection through sensing in a practical FL pipeline. We propose to integrate sensing with communication and computation into a joint design to further boost the communication-and-energy efficiencies of OTA-FL. Specifically, we consider a training latency and energy consumption minimization problem with performance guarantees. To this end, we first derive an *average training error (ATE)* metric to quantify convergence performance. Then, a joint

sensing, communication and computation resource allocation strategy is developed based on a *deep reinforcement learning (DRL)* algorithm that nests convex optimization with a deep Q-network. Extensive experiments are conducted to validate our theoretical analysis, and demonstrate the effectiveness of the proposed design for communication-and-energy efficient FL.

**Index Terms**—Federated learning, over-the-air computation, integrated sensing, computation, communication.

## I. INTRODUCTION

FEDERATED learning (FL) has emerged as a promising technology for enabling edge *artificial intelligence (AI)* in future 6G networks due to its distributed learning framework and privacy-enhancing features [1], [2], [3]. As a result, FL holds significant potential in facilitating large model fine-tuning for edge AI to support emerging intelligent applications, such as *extended reality (XR)*, intelligent transport, intelligent logistics, and digital twin [4], [5]. In the context of edge AI, communication and energy efficiencies are two critical properties that need to be pursued [6], [7], and become increasingly important given the prevalence of large model training. However, communication efficiency and energy efficiency are conflicting objectives, since the improvement of one factor comes at the cost of the other. Recently, *over-the-air FL (OTA-FL)* has emerged as a potential solution to achieve both efficiencies via an integrated communication and computation design by exploiting the superposition property of multi-access channels for fast model aggregation [8], [9].

Prior works on FL have extensively studied the integration of communication and computation, assuming that the data for model training is readily collected and available at each device prior to training [10], [11]. However, in real-world applications, devices continuously acquire and collect new data for model training by sensing their surrounding environment throughout the FL procedure. This indicates that sensing for data acquisition plays a crucial role in the practical FL pipeline, despite being largely overlooked in existing literature [12], [13]. Motivated by this observation, the present work proposes an *integrated sensing, communication and computation (ISCC)* design, in order to advance the limits of communication-and-energy efficient FL [14], [15], [16], [17], [18]. More specifically, the local model at each device is trained based on the streaming data collected through sensing, which significantly impacts both the latency and energy consumption in OTA-FL.

Received 30 May 2024; revised 20 September 2024; accepted 10 November 2024. Date of publication 25 November 2024; date of current version 10 January 2025. This work was supported in part by the National Natural Science Foundation of China under Grant 62293482 and Grant 62371313, in part by the Basic Research Project of Hetao Shenzhen-Hong Kong Science and Technology (HK S&T) Cooperation Zone under Grant HZQB-KCZY-2021067, in part by Shenzhen Outstanding Talents Training Fund under Grant 202002, in part by Guangdong Research Projects under Grant 2017ZT07X152 and Grant 2019CX01X104, in part by Guangdong Provincial Key Laboratory of Future Networks of Intelligence under Grant 2022B121010001, in part by Shenzhen Key Laboratory of Big Data and Artificial Intelligence under Grant ZDSYS201707251409055, in part by Guangdong Major Project of Basic and Applied Basic Research under Grant 2023B0303000001, in part by Guangdong Basic and Applied Basic Research Foundation under Grant 2022A151010109, in part by Shenzhen-Hong Kong-Macau Technology Research Program (Type C) under Grant SGDX20230821091559018, and in part by Longgang District Special Funds for Science and Technology Innovation under Grant LGKCSPT2023002. The associate editor coordinating the review of this article and approving it for publication was M. Giordani. (Corresponding author: Qimei Chen.)

Yipeng Liang, Qimei Chen, and Hao Jiang are with the School of Electronic Information, Wuhan University, Wuhan 430072, China (e-mail: liangyipeng@whu.edu.cn; chenqimei@whu.edu.cn; jh@whu.edu.cn).

Guangxu Zhu is with Shenzhen Research Institute of Big Data, Shenzhen 518172, China (e-mail: gxzhu@sribd.cn).

Yonina C. Eldar is with the Department of Mathematics and Computer Science, Weizmann Institute of Science, Rehovot 7610001, Israel (e-mail: yonina.eldar@weizmann.ac.il).

Shuguang Cui is with the School of Science and Engineering (SSE), Shenzhen Future Network of Intelligence Institute (FNii-Shenzhen), and Guangdong Provincial Key Laboratory of Future Networks of Intelligence, The Chinese University of Hong Kong, Shenzhen 518172, China (e-mail: shuguangcui@cuhk.edu.cn).

Color versions of one or more figures in this article are available at <https://doi.org/10.1109/TWC.2024.3501297>.

Digital Object Identifier 10.1109/TWC.2024.3501297

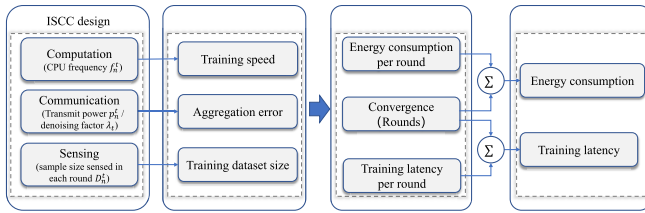


Fig. 1. Illustration of the impact of ISCC design on energy and communication efficiency.

### A. Related Work

Substantial efforts have been devoted to enhancing both energy efficiency and communication efficiency in FL. For example, the authors in [19] proposed an iterative algorithm with low complexity to minimize the energy consumption of FL, by deriving closed-form solutions in each iteration. In [20], energy efficiency of FL under different communication access protocols is examined, where the computation resource for model updating and the communication resource for model transmission are jointly optimized. The paper in [21] investigated an energy consumption minimization problem in Internet of Things networks, by jointly optimizing scheduling, power allocation, and computation frequency allocation. On the other hand, communication-efficient FL has garnered increasing attention as a means to tackle communication overhead [10], [11], [22], [23]. The authors in [10] proposed a joint learning, wireless resource allocation, and user selection scheme for resource-constrained FL. In [11], an adaptive aggregation control algorithm is designed based on data heterogeneity and model features for improved learning performance under limited communication resources. The authors in [22] proposed a FL mechanism for IoT networks based on the unlicensed spectrum technology, where a gradient-norm-value based device selection strategy is suggested to accelerate FL convergence. The work [23] introduced a joint wireless resource allocation and model quantization scheme for communication-efficient FL.

Previous works primarily focus on either energy-efficient or communication-efficient FL, with limited consideration given to achieving both objectives simultaneously. OTA-FL has emerged as a promising solution for communication-and-energy efficient FL in recent years [24], [25], [26], [27], [28]. By exploiting the waveform superposition nature of a wireless multiple-access channel, OTA-FL enables distributed functional computation over the air, leading to benefits of communication efficiency such as reduced latency and enhanced bandwidth efficiency [26]. Specifically, OTA-FL allows multiple devices to simultaneously transmit and aggregate their models on the same time-frequency resources of the uplink channel, thereby enhancing the training efficiency of FL. Nonetheless, OTA-FL suffers from aggregation errors due to channel noise perturbation, which deteriorates FL performance. To address this issue, several approaches have been investigated [29], [30], [31], [32]. For example, power control strategies have been explored in [29] and [30] to reduce aggregation errors. In [31], a Bayesian approach for model aggregation was proposed by exploiting prior distribution of

local weights and channel distribution. The authors in [32] designed a precoding and scaling scheme to mitigate the effect of channel noise, resulting in a convergence rate comparable to that of error-free channels. The authors in [33] proposed a joint transmission probability and local computing control optimization for OTA-FL to minimize the overall energy consumption. However, the works above often overlook the role of sensing by assuming fixed and readily available training datasets throughout the FL process.

### B. Motivation and Contribution

In this paper, we propose a communication-and-energy efficient *OTA-FL with ISCC (OTA-FL-ISCC)* scheme. The proposed framework consists of an edge server and multiple devices, where each device is capable of sensing, communication, and computation abilities [34]. In each communication round, every device performs sensing for sample collection from the surrounding environment. Subsequently, each device trains a local AI model based on the collected data and the on-board computation resource. Then, efficient model aggregation is performed over the air through a wireless channel.

As illustrated in Fig. 1, several pivotal resources of ISCC exert influence over the energy consumption and latency of OTA-FL. Specifically, the CPU cycle frequency, transmit power and denoising factor, and sample size sensed in each communication round respectively determines the training speed, aggregation error, and dataset size. These factors have a cumulative impact on various essential facets of FL, including convergence (i.e., the number of communication rounds required for desired learning performance), energy consumption, and training latency per round. Ultimately, the energy consumption and training latency per round, as well as convergence rate collectively dictate the overall energy and latency of OTA-FL. Consequently, effective ISCC design plays a pivotal role in achieving communication-and-energy efficient OTA-FL.

Hence, we investigate a joint sensing, communication, and computation resource allocation strategy for our proposed OTA-FL-ISCC framework. Specifically, we first derive an *average training error (ATE)* metric to quantify the learning performance by convergence analyses with respect to ISCC resources. Then, a training latency and energy consumption minimization problem with learning performance guarantee is formulated, which is a *mixed integer nonlinear programming (MINLP)* problem. Solving the problem via *deep reinforcement learning (DRL)* yields an efficient strategy for ISCC design.

The main contributions of this work are summarized as follows.

- **Convergence analysis and performance metric:** We investigate the impact of ISCC on the learning performance of OTA-FL-ISCC. We first analyze the convergence performance by taking into account the impact of sample collection and aggregation errors. Thereafter, we quantify this impact via the ATE metric.
- **Communication and energy efficient ISCC:** We formulate a joint ISCC resource optimization problem aimed at minimizing latency and energy consumption for model

training. We decompose the problem into three distinct subproblems: computation resource optimization, communication resource optimization, and sensing resource optimization. The first two subproblems are resolved efficiently by convex optimization techniques. The sensing resource optimization leads itself to a dynamic programming problem, which we address through *deep Q-learning (DQN)*, where the training data for DQN network is derived through communication and computation resource optimizations.

- **Performance evaluation:** We conduct extensive simulations to evaluate our proposed algorithms. Numerical results not only validate our theoretical analyses but also underscore the superior performance of OTA-FL-ISCC in comparison to baselines, including the classic FLs without ISCC design, and OTA-FL-ISCC without optimized resource allocation. Furthermore, our results illustrate the efficiency of our proposed ISCC resource optimization algorithm.

The rest of this paper is organized as follows. Section II introduces the OTA-FL-ISCC mechanism and its system model. In Section III, we theoretically analyze the convergence performance and derive a performance metric. In Section IV, we formulate the optimization problem and design its optimal solutions. Numerical results are presented in Section V followed by a conclusion in Section VI.

Throughout the paper, we use the following notation: We use  $a$  to denote a scalar,  $\mathbf{a}$  is a column vector,  $\mathbf{A}$  is a matrix, and  $|\cdot|$  represents the modulus operator. The Euclidean norm is written as  $\|\cdot\|$ ,  $\langle \mathbf{a}, \mathbf{a}' \rangle$  is the inner product of  $\mathbf{a}$  and  $\mathbf{a}'$ , and  $\mathbb{E}$  represents mathematical expectation.

## II. ARCHITECTURE AND SYSTEM MODEL

In this section, we first introduce the OTA-FL-ISCC scheme by jointly considering sensing, communication, and computation in FL. Thereafter, we respectively present the system model of sensing, communication, and computation.

### A. OTA-FL-ISCC Scheme

In this work, we consider an OTA-FL-ISCC scheme that consists of a single edge server and a set  $\mathcal{N} \triangleq \{1, 2, \dots, N\}$  of  $N$  edge devices to collaboratively train a shared AI model for a specific task, such as, classification and recognition, as shown in Fig. 2. We assume that both the edge server and the devices are equipped with a single antenna for signal transmission. Each device achieves sensing and communication in a time-division manner [12]. In the communication process, all the devices concurrently transmit their own AI models over the same spectrum for efficient model transmission and aggregation. In the sensing process, each device dynamically collects samples of data from the environment for model training.

As shown in Fig. 3, the shared AI model, denoted by  $\mathbf{w} \in \mathbb{R}^q$  with  $q$  being the model size, is trained over  $T$  communication rounds. The training process is to seek a global model  $\mathbf{w}^*$  that satisfies (5), which can be implemented in a distributed manner using the *federated stochastic gradient descent (FedSGD)* algorithm [3]. During each round  $t \in$

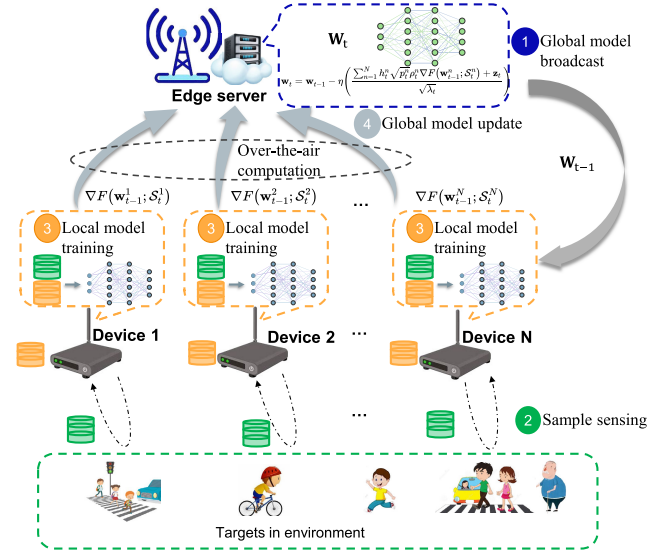


Fig. 2. Illustration of the proposed OTA-FL-ISCC design.

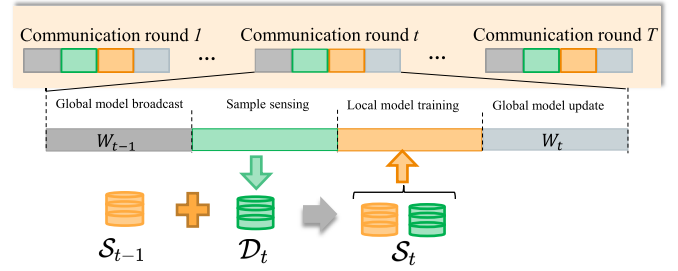


Fig. 3. The procedure of OTA-FL-ISCC in each communication round.

$\mathcal{T} \triangleq \{1, 2, \dots, T\}$ , four steps are performed as elaborated as follows:

- (1) **Global model broadcast:** The edge server broadcasts the global model  $\mathbf{w}_{t-1}$  to all edge devices. Then, each device  $n$  renews its local model  $\mathbf{w}_t^n$  based on the received  $\mathbf{w}_{t-1}$ .
- (2) **Sample sensing:** Each device  $n$  performs a sensing process to collect a new dataset  $\mathcal{D}_t^n$  with a size denoted as  $D_t^n = |\mathcal{D}_t^n|$ . By controlling the sample size  $D_t^n$  in each communication round, OTA-FL-ISCC has the potential to reduce the energy and latency in model training.
- (3) **Local model training:** Each device conducts local training to compute its gradient. Due to the sensing process, each device  $n$  performs local AI model training  $\mathbf{w}_t^n$  based on the accumulated dataset  $\mathcal{S}_t^n$  that includes the newly sensed dataset  $\mathcal{D}_t^n$  from the current communication round  $t$  and the cumulative dataset  $\mathcal{S}_{t-1}^n = \sum_{i=1}^{t-1} \mathcal{D}_i^n$  in the  $(t-1)$ -th communication round, i.e.,  $\mathcal{S}_t^n = \mathcal{D}_t^n + \mathcal{S}_{t-1}^n$ . Define  $F(\mathbf{w}_t^n; \mathcal{S}_t^n)$  as the loss function for device  $n$  over dataset  $\mathcal{S}_t^n$ , which can be given as

$$F(\mathbf{w}_t^n; \mathcal{S}_t^n) = \frac{1}{S_t^n} \sum_{(\mathbf{x}_j, y_j) \in \mathcal{S}_t^n} f(\mathbf{w}_t^n, (\mathbf{x}_j, y_j)), \quad (1)$$

where  $(\mathbf{x}_j, y_j)$  is the  $j$ -th sample of dataset  $\mathcal{S}_t^n$  with data  $\mathbf{x}_j$  and label  $y_j$ . Here  $f(\mathbf{w}_t^n, (\mathbf{x}_j, y_j))$  is the  $j$ -th sample-wise loss function,  $S_t^n = |\mathcal{S}_t^n|$  is the size of dataset  $\mathcal{S}_t^n$ , and  $\mathcal{S}_t^n = \mathcal{S}_{t-1}^n + \mathcal{D}_t^n$ . Subsequently, the local



gradient  $\nabla F(\mathbf{w}_{t-1}^n; \mathcal{S}_t^n)$  can be computed based on the accumulated dataset  $\mathcal{S}_t^n$ .

- (4) **Global model update:** Once all devices have calculated their respective local gradients, they transmit these gradients to the edge server for aggregation, leading to the aggregated gradient as

$$\nabla F(\mathbf{w}_{t-1}; \mathcal{S}_t) = \sum_{n=1}^N \rho_t^n \nabla F(\mathbf{w}_{t-1}^n; \mathcal{S}_t^n). \quad (2)$$

Here  $\mathcal{S}_t$  with size  $S_t = \sum_{n=1}^N S_t^n$  is the accumulated datasets over  $N$  devices at the  $t$ -th communication round, and  $\rho_t^n = \frac{S_t^n}{S_t}$ . Then, the edge server updates the global model based on the aggregated gradient in (2), via

$$\mathbf{w}_t = \mathbf{w}_{t-1} - \eta \nabla F(\mathbf{w}_{t-1}; \mathcal{S}_t), \quad (3)$$

where  $\eta$  is the learning rate. As a result, the global loss function at the  $t$ -th communication round is

$$F(\mathbf{w}_t; \mathcal{S}_t) = \sum_{n=1}^N \rho_t^n F(\mathbf{w}_t^n; \mathcal{S}_t^n). \quad (4)$$

The four steps iteratively repeat over communication rounds until convergence, optimizing the model parameter  $\mathbf{w}$  to minimize the global loss function:

$$\mathbf{w}^* \triangleq \arg \min_{\mathbf{w}} F(\mathbf{w}_T; \mathcal{S}_T). \quad (5)$$

### B. Sensing Model

In the proposed sensing model, we aim to provide a general framework for analyzing the impact of sensing on the proposed federated learning, rather than specific sensing methods.

During sample sensing in every communication round, each device  $n$  dynamically collects datasets  $\mathcal{D}_t^n$  with a designated size of  $D_t^n$ . The learning performance (i.e., classification error) depends significantly on the volume of training samples [35]. Therefore, we introduce the following constraint

$$\sum_{t=1}^T D_t^n \geq S_{tot}^n, \quad (6)$$

where  $S_{tot}^n$  is the dataset size requirement for device  $n$ .

The diverse strategies employed for sample collection ( $D_t^n$  in each communication round) exert a substantial influence on the convergence of FL, which also affects learning performance. Moreover, these diverse strategies in the sensing process have repercussions on the latency and energy consumption of FL. Consequently, the strategic optimization of  $D_t^n$  provides significant potential for enhancing the efficiency of FL.

### C. Communication Model

We consider over-the-air aggregation in the communication process for fast gradient aggregation. Let  $\hat{h}_t^n$  be the complex channel coefficient between device  $n$  and the edge server in the  $t$ -th communication round. As a result, each device can estimate the magnitude  $h_t^n = |\hat{h}_t^n|$  of the channel. In this way,

the received signal at the edge server after phase compensation is expressed as

$$\mathbf{y}_t^{\text{comm}} = \sum_{n=1}^N h_t^n \sqrt{p_t^n} \rho_t^n \nabla F(\mathbf{w}_{t-1}^n; \mathcal{S}_t^n) + \mathbf{z}_t, \quad (7)$$

where  $p_t^n$  represents the transmit power of device  $n$ . Here,  $\mathbf{z}_t \in \mathbb{R}^q$  denotes additive white Gaussian noise, i.e.,  $\mathbf{z}_t \sim \mathcal{CN}(0, \sigma_z^2 \mathbf{I})$ . To achieve over-the-air aggregation, each element of the gradient parameters is modulated as a single analog symbol for transmission. Consequently, a total of  $q$  analog symbols, corresponding to the gradient size of each device, are transmitted. As a result, the transmission latency and energy consumption in the  $t$ -th communication round can be respectively expressed as

$$t_t^{\text{comm}} = \text{ceil} \left( \frac{q}{L_0} \right) T_{\text{slot}}, \quad (8)$$

and

$$e_t^{n, \text{comm}} = p_t^n t_t^{\text{comm}}, \quad (9)$$

where  $L_0$  is the number of symbols in each resource block,  $T_{\text{slot}}$  signifies the duration of each resource block, and  $\text{ceil}(\cdot)$  is the integer ceiling function.<sup>1</sup>

To mitigate the effect of noise on the gradient during wireless transmission, a noise denoising factor  $\lambda_t$  is applied at receiver [29], [30]. Hence, the received global gradient at the edge server is given by

$$\nabla F(\mathbf{w}_{t-1}; \mathcal{S}_t) = \frac{\sum_{n=1}^N h_t^n \sqrt{p_t^n} \rho_t^n \nabla F(\mathbf{w}_{t-1}^n; \mathcal{S}_t^n) + \mathbf{z}_t}{\sqrt{\lambda_t}}. \quad (10)$$

Due to channel noise, the aggregated global model may encounter model distortion. In this case, we define the aggregation error  $\varepsilon_t$  to quantify the gradient parameter distortion based on (2), which is given by

$$\varepsilon_t = \sum_{n=1}^N \rho_t^n \left( \frac{h_t^n \sqrt{p_t^n}}{\sqrt{\lambda_t}} - 1 \right) \nabla F(\mathbf{w}_{t-1}^n; \mathcal{S}_t^n) + \frac{1}{\sqrt{\lambda_t}} \mathbf{z}_t. \quad (11)$$

### D. Computation Model

During  $t$ -th communication round, each device  $n$  conducts local model training using its dataset  $\mathcal{S}_t^n$ . Let  $\xi_t^n$  be the number of CPU cycles required for device  $n$  to execute a single data sample. Furthermore, let  $f_t^n$  represent the CPU-cycle frequency of device  $n$ , while  $\varsigma_t^n$  indicates the energy consumption coefficient specific to the chip of device  $n$ . As a result, the computation latency of device  $n$  is expressed as

$$t_t^{n, \text{comp}} = \frac{\xi_t^n \sum_{i=1}^t D_i^n}{f_t^n} = \frac{\xi_t^n S_t^n}{f_t^n}. \quad (12)$$

<sup>1</sup>In LTE systems, a resource block with duration of  $T_{\text{slot}} = 1$  ms, consists of two slots with 14 symbols. Thus, we have  $L_0 = 14$  [37].

The energy consumption of device  $n$  for computation can be expressed as [19]

$$e_t^{n,\text{comp}} = \xi^n \varsigma^n (f_t^n)^2 \sum_{i=1}^t D_i^n = \xi^n \varsigma^n (f_t^n)^2 S_t^n. \quad (13)$$

In this work, we assume that the latency for each device to sense a sample is constant, as described in [12] and [36]. Therefore, once  $S_{\text{tot}}^n$  is fixed, the latency of the total samples sensed by each device  $n$  remains unchanged and can be ignored in this work. With the detailed models of sensing, communication, and computation at hands, we are interested in the ISCC design problem targeting communication-and-energy efficient FL algorithm, as elaborated in the sequel.

### III. CONVERGENCE ANALYSIS AND PERFORMANCE EVALUATION

In this section, we analyze the convergence of our proposed OTA-FL-ISCC before delving into the problem formulation. While preliminary research has extensively explored the convergence analysis of OTA-FL (e.g., [30, eq(19)]), these studies have predominantly overlooked the critical aspect of sensing for sample collection, which significantly influences the convergence behavior. Consequently, these analyses do not align with the proposed OTA-FL-ISCC design (as stated in Section II-A). Building upon the analytical framework established in these works, we extend the convergence analysis for the proposed OTA-FL-ISCC by considering the impact of the sample size collected in each round on convergence. We initially investigate the impact of the size of newly collected and accumulated samples on the loss function in each communication round. Subsequently, we establish the convergence of the proposed OTA-FL-ISCC. Through the convergence analysis, we are able to derive an ATE metric that accounts for the sensing process in the learning performance of OTA-FL-ISCC.

#### A. Convergence Analysis

To facilitate the convergence analysis of OTA-FL-ISCC, we introduce the following assumptions for the loss function (4) and gradient (2), which are commonly adopted in FL tasks [8], [11], [30].

*Assumption 1 (L-smoothness):* The loss function,  $F(\mathbf{w}_t; \mathcal{S}_t)$ ,  $\forall t$ , is either continuously differentiable or Lipschitz continuous with a non-negative Lipschitz constant  $L \geq 0$ , which can be formulated as

$$F(\mathbf{w}_t; \mathcal{S}_t) \leq F(\mathbf{v}_t; \mathcal{S}_t) + \langle \nabla F(\mathbf{v}_t; \mathcal{S}_t), (\mathbf{w}_t - \mathbf{v}_t) \rangle + \frac{L}{2} \|\mathbf{w}_t - \mathbf{v}_t\|^2, \forall \mathbf{w}_t, \mathbf{v}_t \in \mathbb{R}^q, \quad (14)$$

where  $\nabla F(\mathbf{v}_t; \mathcal{S}_t)$  denotes the gradient of  $F(\mathbf{v}_t; \mathcal{S}_t)$ .

*Assumption 2 (Gradient Bound):* For any dataset  $\mathcal{S}_t$  at  $t$ -th communication round, the expected squared norm of the gradient  $\nabla F(\mathbf{w}_t; \mathcal{S}_t)$  is bounded by a positive constant  $G_t$ , namely,

$$\mathbb{E}(\|\nabla F(\mathbf{w}_t; \mathcal{S}_t)\|^2) \leq G_t. \quad (15)$$

Recall that since the model parameter vector  $\mathbf{w}_t^n$  is renewed according to the cumulative dataset  $\mathcal{S}_{t-1}^n$  and the newly sensed dataset  $\mathcal{D}_t^n$ , it is essential to discuss the impact of these datasets on the improvement of the global loss function in each communication round.

*Lemma 1:* Given the datasets  $\mathcal{S}_{t-1}^n$  and  $\mathcal{D}_t^n$  in the  $t$ -th communication round, the gradient  $\nabla F(\mathbf{w}_{t-1}; \mathcal{S}_t)$  satisfies the following equation

$$\nabla F(\mathbf{w}_{t-1}; \mathcal{S}_t) = \frac{S_{t-1}}{S_t} \nabla F(\mathbf{w}_{t-1}; \mathcal{S}_{t-1}) + \frac{D_t}{S_t} \nabla F(\mathbf{w}_{t-1}; \mathcal{D}_t), \quad (16)$$

where  $D_t = \sum_{i=1}^N D_t^i$ .

*Proof:*

Please see Appendix A. □

Lemma 1 leads to Lemma 2 which derives an upper bound on the improvement of the global loss function.

*Lemma 2:* When the learning rate  $\eta$  satisfies  $0 \leq \eta \leq \frac{S_{t-1}}{LS_t}$  in the  $t$ -th communication round, the improvement of the global loss function is bounded by (17), as shown at the bottom of the next page.

*Proof:* Please see Appendix B. □

From (17), we obtain several observations: 1) The improvement of the global loss function is related to both the sensing related term (i.e., the size of datasets  $\mathcal{S}_{t-1}$  and  $\mathcal{D}_t$ ) and a communication related term (i.e., aggregation error  $\epsilon_t$ ); 2) The increment of both sensing-related and communication-related terms decreases the improvement of the global loss function, which slows down the OTA-FL-ISCC convergence rate.

The average-squared gradient norm is widely adopted to depict the performance of FL [12]. Based on Lemma 1 and Lemma 2, we introduce the following Theorem to show the upper bound of the average-squared gradient norm.

*Theorem 1:* Under the condition  $0 \leq \eta \leq \frac{S_{t-1}}{LS_t}, \forall t$ , the average-squared gradient norm after  $T$  communication rounds is bounded by

$$\begin{aligned} & \frac{1}{T} \sum_{t=1}^T \|\nabla F(\mathbf{w}_{t-1}; \mathcal{S}_{t-1})\|^2 \\ & \leq \underbrace{\frac{1}{T} \left[ 2G_1 + 3\mathbb{E}(\|\epsilon_1\|^2) \right]}_{\text{Error of 1st communication round}} \\ & \quad + \underbrace{\frac{2(F(\mathbf{w}_0; \mathcal{S}_0) - F^*)}{T\eta}}_{\text{Error of Initialization}} \\ & \quad + \underbrace{\frac{1}{T} \sum_{t=2}^T \left[ \left( 1 + \frac{2D_t}{S_{t-1}} \right) \mathbb{E}(\|\epsilon_1\|^2) + \frac{2D_t}{S_{t-1}} G_t \right]}_{\text{Error of rest communication rounds}}. \quad (18) \end{aligned}$$

From (18), we note that the convergence performance of OTA-FL-ISCC is controlled by sample collection strategy (i.e., the size of dataset collected in each communication round) and aggregation errors. To achieve a better OTA-FL-ISCC performance, we can decrease the upper bound of (18) by optimizing the sample collection strategy and reducing aggregation errors. These results provide guidance for the

design of resource allocation algorithms in the subsequent section.

### B. Performance Metric

Although (18) presents an upper bound on the average squared gradient norm, it cannot be directly used to depict the OTA-FL-ISCC performance due to the undetermined values of  $L$  and  $F^*$ . We assume that the gradient parameters to be transmitted follow the standard normal distribution, which can be achieved as referenced in [8]. According to (11), the corresponding instantaneous *mean square error (MSE)* of aggregation errors at the  $t$ -th round is given by

$$\begin{aligned} & \mathbb{E} \|\epsilon_t\|^2 \\ & \stackrel{(a)}{\leq} \sum_{n=1}^N \rho_t^n \left( \frac{h_t^n \sqrt{p_t^n}}{\sqrt{\lambda_t}} - 1 \right)^2 \sum_{n=1}^N \rho_t^n \mathbb{E} \|\nabla F(\mathbf{w}_{t-1}^n; \mathcal{D}_t)\|^2 \\ & \quad + \frac{\mathbb{E} \|\mathbf{z}_t\|^2}{\lambda_t} \\ & \stackrel{(b)}{=} q \left[ \sum_{n=1}^N \rho_t^n \left( \frac{h_t^n \sqrt{p_t^n}}{\sqrt{\lambda_t}} - 1 \right)^2 + \frac{\sigma_z^2}{\lambda_t} \right], \end{aligned} \quad (19)$$

where (a) is derived from the Cauchy-Schwarz inequality, and (b) is obtained based on the distribution of  $\nabla F(\mathbf{w}_{t-1}^n; \mathcal{D}_t)$  and  $\mathbf{z}_t$ . As a result, (18) can be further expressed as

$$\begin{aligned} \frac{1}{T} \sum_{t=1}^T \|\nabla F(\mathbf{w}_{t-1}; \mathcal{S}_{t-1})\|^2 & \leq \frac{2(F(\mathbf{w}_0; \mathcal{S}_0) - F^*)}{T\eta} \\ & \quad + \frac{2G_1}{T} + \frac{q}{T} \sum_{t=1}^T \phi_t. \end{aligned} \quad (20)$$

Here,  $\phi_t$  is given by (21), as shown at the bottom of the next page, where  $\bar{G}_t = \frac{G_t}{q}$ . Therefore, we can define the ATE metric as

$$\Phi = \frac{1}{T} \sum_{t=1}^T \phi_t. \quad (22)$$

### C. Computational Complexity and Scalability Assessment

In this subsection, we analyze the computational complexity and scalability of the proposed OTA-FL-ISCC framework. To facilitate the analysis, we set  $\rho_t^n = \frac{1}{N}$ . According to (19) and (22), the expected ATE is given by

$$\mathbb{E}(\Phi) = \frac{1}{T} \sum_{t=2}^T \left( \frac{2D_t}{S_{t-1}} \right) \bar{G}_t$$

$$\begin{aligned} & + \frac{1}{qT} \mathbb{E} \left[ 3 \|\epsilon_1\|^2 + \sum_{t=2}^T \left( 1 + \frac{2D_t}{S_{t-1}} \right) \|\epsilon_t\|^2 \right] \\ & = \frac{3}{NT} \left( \frac{h_1^n \sqrt{p_1^n}}{\sqrt{\lambda_t}} - 1 \right)^2 + \frac{1}{T} \sum_{t=2}^T \frac{2D_t}{S_{t-1}} \bar{G}_t + \frac{M}{NT}, \end{aligned} \quad (23)$$

where

$$M = \sum_{t=2}^T \left[ \left( 4 + \frac{2D_t}{S_{t-1}} \right) \frac{\sigma_z^2}{\lambda_t} + \left( 1 + \frac{2D_t}{S_{t-1}} \right) \left( \frac{h_t^n \sqrt{p_t^n}}{\sqrt{\lambda_t}} - 1 \right)^2 \right].$$

It is evident that the first term on the right side of equation (23) represents the aggregation errors of the 1st communication round, which tends to converge to zero as  $T \rightarrow \infty$ . The second term is associated with the sample sensing strategy, while the last term pertains to both communication errors and sample sensing strategy. From (23), we can derive the computational complexity of our proposed framework as  $\mathbb{E}(\Phi) = \mathcal{O} \left( \frac{M}{NT} + \frac{1}{T} \sum_{t=2}^T \frac{2D_t \bar{G}_t}{S_{t-1}} \right)$ .

To analyze the scalability of our proposed federated learning framework, we let  $N \rightarrow \infty$  to (23). It is observed that the first term of (23) converges to zero as  $N \rightarrow \infty$ , whereas the second term remains independent of the device count  $N$ , serving as an error floor for scalability. The last term is influenced by aggregation errors and sample sensing strategy. Therefore, scalability can be enhanced by optimizing aggregation errors and sample sensing strategy.

## IV. PROBLEM FORMULATION AND OPTIMIZATION

Based on the system model and convergence results, we are ready to formulate a training latency and energy consumption minimization problem to achieve a communication-and-energy efficient FL. Thereafter, a joint sensing, communication and computation resource allocation strategy is proposed to address the optimization problem.

### A. Problem Formulation

Our design objective is to minimize the long-term average communication-and-energy efficient FL, which addresses both the energy consumption and the latency in model training. Therefore, the problem is formulated as

$$\mathcal{P}1 : \min_{\{\mathcal{D}, f, p, \lambda\}} \lim_{T \rightarrow \infty} \frac{1}{T} \sum_{t=1}^T \mathbb{E}[e_t + wt_t], \quad (24)$$

$$\text{s.t. } D_t^n \in \mathbb{N}, \quad \forall n, t, \quad (24a)$$

$$\begin{aligned} & F(\mathbf{w}_t; \mathcal{S}_t) - F(\mathbf{w}_{t-1}; \mathcal{S}_{t-1}) \\ & \leq \begin{cases} \underbrace{-\frac{\eta}{2} \mathbb{E} \left( \|\nabla F(\mathbf{w}_0; \mathcal{S}_0)\|^2 \right)}_{\text{sensing related term}} + \underbrace{\frac{3\eta}{2} \mathbb{E} \left( \|\epsilon_1\|^2 \right)}_{\text{communication related term}}, & \text{if } t = 1, \\ \underbrace{-\frac{\eta}{2} \mathbb{E} \left( \|\nabla F(\mathbf{w}_{t-1}; \mathcal{S}_{t-1})\|^2 \right)}_{\text{sensing related term}} + \underbrace{\frac{G_t \eta}{2} \frac{2D_t}{S_{t-1}}}_{\text{sensing \& communication related term}} + \underbrace{\frac{\eta}{2} \left( 1 + \frac{2D_t}{S_{t-1}} \right) \mathbb{E} \left( \|\epsilon_t\|^2 \right)}_{\text{sensing \& communication related term}}, & \text{otherwise.} \end{cases} \end{aligned} \quad (17)$$

$$\sum_{t=1}^T D_t^n \geq S_{\text{tot}}^n, \quad \forall n, \quad (24b)$$

$$\Phi \leq \delta, \quad (24c)$$

$$0 \leq p_t^n \leq p_{\max}^n, \quad \forall n, t, \quad (24d)$$

$$0 \leq f_t^n \leq f_{\max}^n, \quad \forall n, t, \quad (24e)$$

$$\lambda_t \geq 0, \quad \forall t, \quad (24f)$$

where  $\mathbf{D} = [D_1^1, \dots, D_T^N]^T$ ,  $\mathbf{f} = [f_1^1, \dots, f_T^N]^T$ ,  $\mathbf{p} = [p_1^1, \dots, p_T^N]^T$ ,  $\boldsymbol{\lambda} = [\lambda_1, \dots, \lambda_T]^T$  represent sample size, CPU frequency, transmit power, and denoising factor variables, respectively. Here,  $t_t = \max_{n \in \mathcal{N}} \{t_t^{n, \text{comp}}\} + t_t^{\text{comm}}$  and  $e_t = \sum_{n=1}^N (e_t^{n, \text{comp}} + e_t^{n, \text{comm}})$  are the energy and latency in  $t$ -communication round.  $w$  is a weighting factor to keep balance between latency and energy consumption in OTA-FL-ISCC.  $S_{\text{tot}}^n$  in (24b) is the dataset size requirement for device  $n$ .  $\delta$  in (24c) is the threshold for performance constraint.  $p_{\max}^n$  in (24d) is the maximum transmit power constraint for each device.  $f_{\max}^n$  in (24e) is the constraint on computational frequency of device  $n$ .

$\mathcal{P}1$  is an MINLP and non-convex problem, which is challenging to solve. A joint sensing, communication and computation resource allocation strategy is designed in the next subsection.

### B. Joint Sensing, Communication and Computation Resource Allocation Strategy

Intuitively,  $\mathcal{P}1$  can be divided into three subproblems: sensing, computation, and communication resource allocation. Specifically, we utilize convex optimization methods to solve the computation and communication resource allocation subproblems under given  $\mathbf{D}^*$ . We adopt the DQN algorithm to deal with the sensing resource allocation subproblem given  $\mathbf{f}^*$ ,  $\mathbf{p}^*$ , and  $\boldsymbol{\lambda}^*$ . We first present the optimization methods for computation and communication resource allocation, respectively. Subsequently, we introduce the DQN algorithm for addressing the sensing resource allocation subproblem. Finally, we present the overall design of the DRL-based algorithm along with a complexity analysis.

1) *Computation Resource Allocation*: Given sensing and communication resource allocation, the computation resource allocation subproblem is expressed as

$$\mathcal{P}2 : \min_{\{\mathbf{f}\}} \lim_{T \rightarrow \infty} \frac{1}{T} \sum_{t=1}^T \mathbb{E} \left[ \sum_{n=1}^N e_t^{n, \text{comp}} + w \max_{n \in \mathcal{N}} \{t_t^{n, \text{comp}}\} \right], \quad (25)$$

subject to (24e).

Note that  $\mathcal{P}2$  is independent to the communication rounds. Therefore, it can be decomposed into  $T$  separated subproblems, each addressed independently. Without loss of generality,

the computation resource allocation subproblem for communication round  $t$  is formulated as

$$\mathcal{P}2.1 : \min_{\mathbf{f}} \left\{ \sum_{n=1}^N e_t^{n, \text{comp}} + w \max_{n \in \mathcal{N}} \{t_t^{n, \text{comp}}\} \right\}, \quad (26)$$

subject to (24e).

To solve  $\mathcal{P}2.1$ , we introduce an auxiliary variable  $\chi^t$  to represent the maximum computation latency among the devices. Then,  $\mathcal{P}2.1$  can be rearranged as

$$\begin{aligned} \mathcal{P}2.2 : \min_{\mathbf{f}} \left\{ \sum_{n=1}^N e_t^{n, \text{comp}} + w \chi_t \right\}, \quad (27) \\ \text{s.t. (24e),} \\ \chi_t \geq t_t^{n, \text{comp}}, \quad \forall n. \end{aligned} \quad (27a)$$

$\mathcal{P}2.2$  is a convex problem. To solve it, the Lagrange method is employed. Specifically, we define the Lagrangian as

$$\begin{aligned} \mathcal{L}(\{f_t^n\}, \chi_t, \mu_n) = \sum_{n=1}^N \xi_n \varsigma_n S_t^n (f_t^n)^2 \\ + w \chi_t + \sum_{n=1}^N \mu_n \left( \frac{\xi_n S_t^n}{f_t^n} - \chi_t \right), \end{aligned} \quad (28)$$

where  $\mu_n \geq 0$  is the Lagrange multiplier related to (27a). Intuitively, (28) is a convex function to  $f_t^n$  and  $\chi_t$ . Taking the first-order derivation of (28) with respect to  $f_t^n$  and setting it to 0, we have  $f_t^{n*} = \sqrt[3]{\frac{\mu_n^*}{2\varsigma_n}}$ . Here  $\mu_n^*$  is the optimal Lagrange multiplier. Combining (24e), the optimal computation resource allocation is given by

$$f_n^{t*} = \min \left[ \sqrt[3]{\frac{\mu_n^*}{2\varsigma_n}}, f_n^{\max} \right], \quad \forall n \in \mathcal{N}. \quad (29)$$

2) *Communication Resource Allocation*: Given the sensing and computation resource allocation, the communication resource allocation subproblem is degenerated into a communication energy minimization problem, which can be expressed as

$$\mathcal{P}3 : \min_{\{\mathbf{p}, \boldsymbol{\lambda}\}} \lim_{T \rightarrow \infty} \frac{1}{T} \sum_{t=1}^T \mathbb{E} \left[ \sum_{n=1}^N e_t^{n, \text{comm}} \right], \quad (30)$$

subject to (24c), (24d), and (24f).

Note that  $\mathcal{P}3$  is constrained by the ATE metric, which encompasses  $T$  communication rounds in equation (24c). This makes it challenging to solve independently for each communication round  $t$ , thereby leading to difficulties in integrating it with the DQN algorithm. To tackle this issues, we relax (24c) by

$$\phi_t \leq \delta, \quad \forall t. \quad (31)$$

$$\phi_t = \begin{cases} 3 \left[ \sum_{n=1}^N \rho_t^n \left( \frac{h_t^n \sqrt{p_t^n}}{\sqrt{\lambda_t}} - 1 \right)^2 + \frac{\sigma_z^2}{\lambda_t} \right], & \text{if } t = 1, \\ \left( 1 + \frac{2D_t}{S_{t-1}} \right) \left[ \sum_{n=1}^N \rho_t^n \left( \frac{h_t^n \sqrt{p_t^n}}{\sqrt{\lambda_t}} - 1 \right)^2 + \frac{\sigma_z^2}{\lambda_t} \right] + \frac{2D_t}{S_{t-1}} \bar{G}_t, & \text{otherwise,} \end{cases} \quad (21)$$



Consequently,  $\mathcal{P}3$  can be decomposed into  $T$  independent subproblems. Specifically, the communication resource allocation problem for each  $t$  is formulated as

$$\begin{aligned} \mathcal{P}3.1 : \min_{\{p, \lambda\}} & \sum_{n=1}^N e_t^{n, \text{comm}}, \\ \text{s.t. } & (24d), (24f), \\ & \sum_{n=1}^N \rho_t^n \left( \frac{h_t^n \sqrt{p_t^n}}{\sqrt{\lambda_t}} - 1 \right)^2 + \frac{\sigma_z^2}{\lambda_t} \leq \bar{\delta}_t, \quad \forall t, \end{aligned} \quad (32)$$

$$(32a)$$

where  $\bar{\delta}_t$  is given by

$$\bar{\delta}_t = \begin{cases} \frac{\delta}{2 + \eta}, & t = 1, \\ \frac{\delta_t - \left[ \frac{D_t}{S_t} + \frac{D_{t-1}}{S_{t-1}} \left( 1 + \frac{D_t}{S_t} \right) \right] \bar{G}_t}{1 + \frac{2D_t}{S_{t-1}}}, & \text{otherwise.} \end{cases} \quad (33)$$

Note that (31) is a more stringent constraint than that in (24c). Therefore, any solution to problem  $\mathcal{P}3.1$  become automatically a solution to problem  $\mathcal{P}3$ . Consequently, we can achieve at least a feasible yet sub-optimal solution for  $\mathcal{P}3$  by solving  $\mathcal{P}3.1$ . It is noteworthy that the typical approach of alternating optimization for solving  $\mathcal{P}3.1$  exhibits high computational complexity of  $\mathcal{O}(N^{3.5})$ . To overcome the issue and inspired by [24] and [39], we proposed a novel communication resource allocation method with reduced computation complexity of  $\mathcal{O}(N \log N)$  [29]. Moreover, this method provides a closed-form expression, facilitating its subsequent integration with the DQN algorithm.

Without loss of generality, we assume that the channel coefficients satisfy the ordering property:  $h_t^1 \leq h_t^2 \leq \dots \leq h_t^N$ . According to the channel inversion policy [24], the instantaneous transmission power of device  $n$  is given as

$$\sqrt{p_t^n} = \begin{cases} \sqrt{p_{\max}^n}, & 1 \leq n < m, \\ \frac{\sqrt{\lambda_t}}{h_t^n}, & m \leq n \leq N, \end{cases} \quad (34)$$

where  $m \in \mathcal{N}$  is the number of devices with maximum transmission power. According to (34), we can easily derive the optimal denoising factor  $\lambda_t^*$  for any given  $m$ . Specifically, by taking the first order derivative of  $\sum_{n=1}^N \rho_t^n \left( \frac{h_t^n \sqrt{p_t^n}}{\sqrt{\lambda_t}} - 1 \right)^2 + \frac{\sigma_z^2}{\lambda_t}$  and setting it to zero, we have

$$\lambda_t^* = \frac{\sum_{i=0}^m \rho_t^i \sqrt{p_{\max}^i} h_t^i}{\sum_{i=0}^m \rho_t^i p_{\max}^i (h_t^i)^2 + \sigma_z^2}, \quad \forall t. \quad (35)$$

Consequently, the optimal power allocation can be further obtained by

$$\sqrt{p_t^{n*}} = \begin{cases} \sqrt{p_{\max}^n}, & 1 \leq n < m, \\ \frac{\sqrt{\lambda_t^*}}{h_t^n}, & m \leq n \leq N. \end{cases} \quad (36)$$

As a result, given (35) and (36), we can solve  $\mathcal{P}3.1$  by determining the optimal value of  $m$ ,  $\forall m \in \mathcal{N}$ . To this end, we first

define the communication energy consumption corresponding to  $m$  as  $V_m = \sum_{n=1}^N e_t^{n, \text{comm}*}$ . Next, we define  $\mathcal{M}$  as the set containing the communication energy consumption values  $V_m$  for all candidate values of  $m$ . Therefore, to determine the optimal value of  $m$ , we only need to compare the energy consumption values within the set  $\mathcal{M}$ ,

$$m^* = \arg \min_{m \in \mathcal{M}} V_m. \quad (37)$$

3) *Sensing Resource Allocation*: Given communication and computation resource allocation, the sensing resource allocation optimization subproblem is presented as

$$\mathcal{P}4 : \min_{\{D\}} \lim_{T \rightarrow \infty} \frac{1}{T} \sum_{t=1}^T \mathbb{E} [e_t^{n, \text{comp}} + w t_t^{n, \text{comp}}], \quad (38)$$

$$\text{s.t. } (24a), (24b), (32a). \quad (38a)$$

Note that the sensing resource allocation subproblem is essentially a dynamic programming (time series) problem due to the accumulating samples across communication rounds. DRL has been widely adopted as an efficient algorithm to solve decision-making problems by learning optimal solutions in dynamic environments [38]. To apply this method, we first reformulate the subproblem as a MDP with a tuple  $\langle \mathcal{S}, \mathcal{A}, \mathcal{P}, \mathcal{R} \rangle$ , where  $\mathcal{S}$ ,  $\mathcal{A}$ ,  $\mathcal{P}$ , and  $\mathcal{R}$  are the state space, action space, state transition probability, and reward, respectively. The corresponding elements in the tuple are presented as follows.

- State space  $\mathcal{S}$ . In the  $t$ -th communication round,  $\mathbf{s}_t$  consists of the accumulative dataset size  $S_{t-1}^n$  and the channel coefficient  $h_t^n$  as  $\mathbf{s}_t = \{S_{t-1}^n, h_t^n\}_{n \in \mathcal{N}}$ .
- Action space  $\mathcal{A}$ . We define the sample size  $D_t^n$  as  $\mathbf{a}_t$ . However, if each device  $n$  independently selects its own sample size  $D_t^n$ , its action space size is unacceptable. Therefore, we allow all the devices to select the same sample size  $\bar{D}_t$  in the  $t$ -th communication round, i.e.,  $D_t^n = \bar{D}_t, \forall n$ . In this case, we have the action space  $\mathbf{a}_t = \{\bar{D}_t | \bar{D}_t \in \mathbb{N}\}$ .
- State transition probability  $\mathcal{P}$ . Let  $\mathcal{P}(s_{t-1} | s_t, \mathbf{a}_t)$  be the probability of transitioning from state  $s_{t-1}$  to state  $s_t$  under action  $\mathbf{a}_t$ .
- Reward  $\mathcal{R}$ . Reward  $r_t$  is designed to evaluate the quality of a learning policy under state-action pair  $(\mathbf{s}_t, \mathbf{a}_t)$ , which is defined as

$$\begin{aligned} r_t(\mathbf{s}_t, \mathbf{a}_t) = & -(e_t + w t_t) + \alpha \sum_{i=1}^t \bar{D}_i \\ & - 2\beta \left( u(\phi_t - \delta_t) - \frac{1}{2} \right), \end{aligned} \quad (39)$$

where  $\alpha$  and  $\beta$  are the penalty factors for constraints (24b) and (24c), respectively.  $u(\cdot)$  is a unit step function.

Then, the MDP can be formulated with the tuple above. Specifically, we first define a policy  $\pi(\mathbf{a}_t | \mathbf{s}_t)$  as the probability of taking action  $\mathbf{a}_t$  at the state  $\mathbf{s}_t$ , i.e.,  $\pi(\mathbf{a}_t | \mathbf{s}_t) = \mathcal{P}(\mathbf{a}_t | \mathbf{s}_t)$ . Moreover, the discounted reward function is defined as

$$U_t = \lim_{T \rightarrow +\infty} \sum_{i=t}^T \gamma^{i-t} r_i(\mathbf{s}_i, \mathbf{a}_i), \quad (40)$$



where  $\gamma \in (0, 1]$  is the discount factor for weighting future rewards. The goal of the agent is to find the optimal policy  $\pi^*$  that maximizes the expected long-term rewards  $\mathbb{E}_{\pi^*}[U_t]$ . To this end, DQN algorithm is utilized. Specifically, under a certain policy  $\pi$ , the state-action function  $Q^\pi(s_t, a_t; \theta)$  is defined as the expected future long-term reward for a state-action pair  $(s_t, a_t)$ , which is presented by

$$Q^\pi(s_t, a_t; \theta) = \mathbb{E}_\pi[U_t | s_t, a_t], \quad (41)$$

where  $\theta$  is the parameter vector of the Q-network.

To find the optimal policy  $\pi^*$ , we need to obtain the optimal action-value function  $Q^*(s_t, a_t; \theta)$ , which can be achieved through the Bellman equation as

$$Q^*(s_t, a_t; \theta) = r_t + \gamma \max_{a_{t+1}} Q^*(s_{t+1}, a_{t+1}; \theta). \quad (42)$$

Note that the optimal action-value function  $Q^*$  can be obtained by optimizing the parameter vector  $\theta$  of the Q-network. To this end, the replay buffer is considered to learn the optimal parameter vector  $\theta$  and improve the efficiency. Specifically, the historical tuple  $(s_t, a_t, r_t, s_{t+1})$  after each interaction between the agent and the environment is stored in the experience replay buffer. By sampling the historical tuples, we aim to minimize the loss function as

$$\mathcal{L}(\theta) = \left[ \left( r_t + \gamma \max_{a_{t+1}} Q(s_{t+1}, a_{t+1}; \hat{\theta}) - Q(s_t, a_t; \theta) \right)^2 \right], \quad (43)$$

where  $\hat{\theta}$  is the target Q-network. A gradient descent method is employed to minimize the loss function  $\mathcal{L}(\theta)$ . As a result, the optimal data collection solution can be achieved by obtaining the optimal parameter vector  $\theta^*$ .

### C. Algorithm Design And Complexity Analysis

Followed by the proposed resource optimization methods, we introduce a joint sensing, communication and computation resource allocation strategy. Specifically, we employ DQN to optimize sample collection strategy after reformulating  $\mathcal{P}4$  as a MDP, integrating communication and computation resource allocation methods. The detailed procedure is shown in Algorithm 1, where we define (39) as the rewards.

## V. SIMULATION RESULTS

In this section, numerical results are conducted to validate the effectiveness of our proposed OTA-FL-ISCC and theoretical analyses, as well as compare the proposed algorithm with benchmarks.

### A. Experiment Setup

We consider an OTA-FL-ISCC mechanism consists of an edge server and  $N = 10$  devices to jointly learn a *convolutional neural network (CNN)* model for target classification/recognition. We evaluated the local training model on two different datasets: the MNIST and the fashion MNIST datasets.

### Algorithm 1 Algorithm for $\mathcal{P}1$ via the Joint Sensing, Communication and Computation Resource Allocation Strategy

**Input:** Initialize parameter vector of Q-networks  $\theta^1$ ;  
Initialize the experience buffer; Maximum episode number  $L_{\max}$ .

```

1 for episode  $\ell = 1$  to  $L_{\max}$  do
2   Reset the initial state  $s_1$ ;
3   for communication round  $t = 1$  to  $T$  do
4     DQN agent selects discrete action  $a_t$  based on the observed state  $s_t$ ;
5     Obtain the optimal  $f_t^{n*}$  by resolving  $\mathcal{P}2$ ;
6     Obtain the optimal  $p_t^{n*}$  and  $\lambda_t^*$  by resolving  $\mathcal{P}3.1$ ;
7     Calculate the reward  $r_t$  with  $f_t^{n*}$ ,  $p_t^{n*}$  and  $\lambda_t^*$ ;
8     Observe the next  $s_{t+1}$ ;
9     Add transition  $(s_t, a_t, r_t, s_{t+1})$  to the replay buffer;
10    Sample a minibatch from the replay buffer;
11    Update DQN network by the gradient descent method:  $\theta^{t+1} \leftarrow \theta^t$ ;
12  end
13 end
```

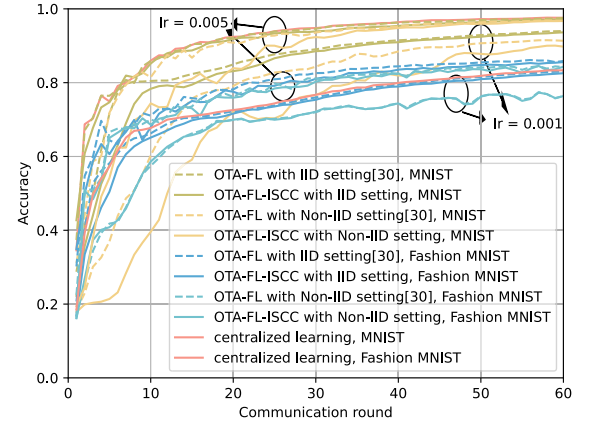


Fig. 4. Performance evaluation under different dataset distribution.

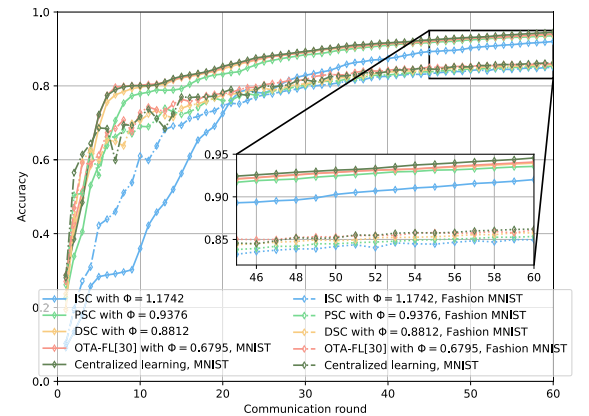


Fig. 5. Performance evaluation over different sensing strategies.

We set the learning rate to 0.001 and the gradient bound to  $G_t = 20490$ . The size of the AI model is  $q = 20490$ .

The CPU-cycle frequency  $f_t^n$  ranges from  $0.1 \times 10^9$  to  $2.0 \times 10^9$ . We further assumed the CPU cycles required for processing one sample is  $\xi^n = 13,876,800$ , and the energy consumption coefficient is  $\varsigma^n = 10^{-28}$ . Moreover, we set the learning performance constraint  $\delta$  and the total sample set size constraint  $S_{\text{tot}}^n$  to 0.95 and 1500, respectively.

We assume that the wireless channels between each device and the edge server follow *independent and identically distributed* (i.i.d.) Rayleigh fading. We assume that the noise variance  $\sigma_z^2 = 1$  W, and the maximum transmit power budget of each device  $P_{\text{max}}^n = 10$  W, if not specified. Moreover, the transmission latency is set as  $t_t^{\text{comm}} = 1.5$  s.

To evaluate our proposed OTA-FL-ISCC mechanism, we introduce the following benchmarks.

- **Centralized learning:** We consider the traditional centralized learning, where all the samples are sensed and gathered by one device or server before model training.
- **OTA-FL [30]:** We consider the classic OTA-FL with gradient aggregation, where all the samples are sensed before the model training.
- **OTA-FL with Fixed Computation Resource (OTA-FL-FCR):** We consider the OTA-FL-FCR, where only the communication resource is optimized.
- **Decrease Sample Collection (DSC):** We consider the proposed OTA-FL-ISCC with DSC strategy, where the sample set size  $D_t$  decreases with the increment of communication rounds.
- **Increase Sample Collection (ISC):** We consider the proposed OTA-FL-ISCC with ISC strategy, where the sample set size  $D_t$  increases with the increment of communication rounds.

### B. Validation of Theoretical Analyses

In Fig. 4, the convergence performance of the proposed OTA-FL-ISCC and OTA-FL schemes are illustrated across different datasets, each with both IID and Non-IID settings. It is evident from the figure that the OTA-FL-ISCC exhibits worse convergence performance than the classic OTA-FL across both the Fashion MNIST and MNIST datasets under both IID and Non-IID settings. For example, although OTA-FL-ISCC and OTA-FL converge after 50 communication rounds, OTA-FL generally achieves higher accuracy than OTA-FL-ISCC under different learning rates. This verifies our theoretical analysis that the sensing-related and communication-related terms have negative impacts on the improvement of global loss in each communication round.

Fig. 5 evaluates the derived performance metric  $\Phi$  over different sample collection strategies, where the PSC denotes the proposed sample collection strategy achieved by Algorithm 1. It can be found that different sample collection strategies would influence the performance of OTA-FL-ISCC. Different sample collection strategies correspond to different value of  $\Phi$ , i.e., ISC has a value of  $\Phi = 1.1742$ , PSC has a value of  $\Phi = 0.9711$ , DSC has a value of  $\Phi = 0.8812$ , and OTA-FL has a value of  $\Phi = 0.6795$ . According to Fig. 5, a smaller value of  $\Phi$  leads to higher accuracy, which verifies our theoretical analyses that a better learning performance can be achieved by minimizing the ATE  $\Phi$ .

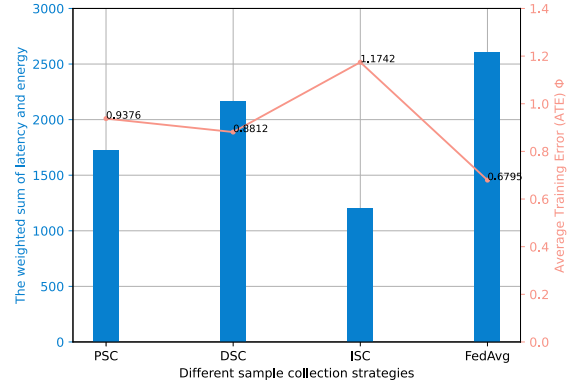


Fig. 6. The ATE and the weighted sum of latency and energy over different sample sensing strategies.

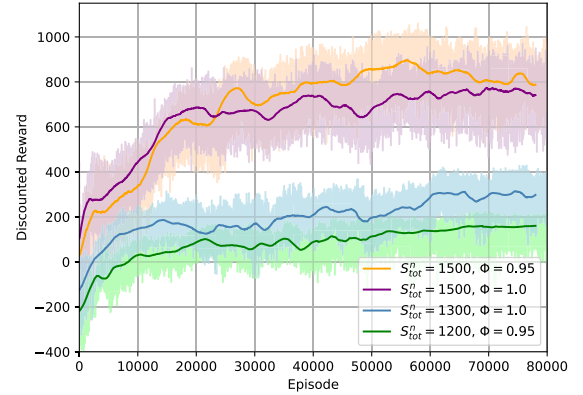


Fig. 7. The convergence performance of Algorithm 1.

Fig. 6 further presents the performance of weighted training latency and energy consumption, as well as the ATE over different sample collection strategies. Here, all the strategies are all under optimal communication and computation resource allocation. Intuitively, the OTA-FL scheme leads to the highest weighted sum of training latency and energy consumption but lowest ATE, since it needs to update the local model over all the dataset  $S_{\text{tot}}^n$  in each communication round. However, the proposed OTA-FL-ISCC can still achieve better performance by optimizing the sample collection strategy with low latency and energy consumption, which indicates effectiveness on reducing the latency and energy consumption for training a AI model at edge networks.

### C. Effectiveness of the Proposed Algorithms

Fig. 7 demonstrates the efficiency of the proposed Algorithm 1 under various constraints. It is observed that the discounted rewards converges within 80000 episodes under different constraints. Furthermore, it is also observed that the discounted reward converges to different points according to different datasize and ATE, highlighting its effectiveness. For instance, when  $\phi = 0.95$ , the reward with a datasize of 1500 significantly surpasses that with a datasize of 1200, emphasizing the impact of the constraint of larger dataset size.

In Fig. 8, we depict the convergence from a weighted sum of energy and latency perspectives under various schemes, each

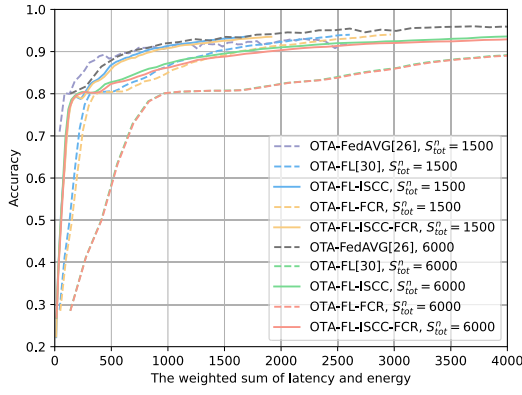


Fig. 8. The weighted sum of energy and latency VS convergence.

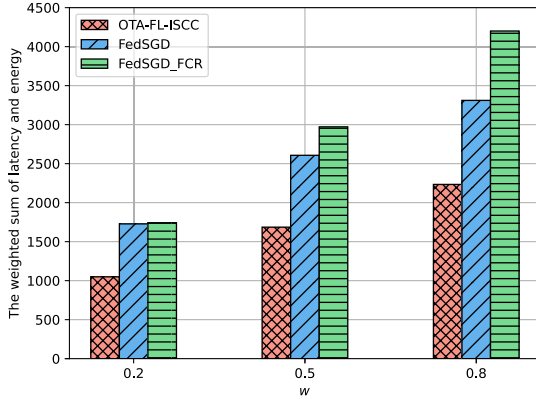


Fig. 9. The weighted sum of training latency and energy consumption over different schemes.

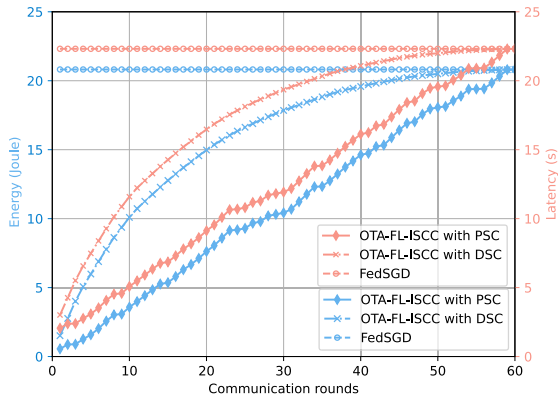


Fig. 10. The energy consumption and latency in each communication round.

with different settings for  $S_{tot}^n$ , to showcase the effectiveness of our design for communication-and-energy efficient OTA-FL. It is evident that the convergence of the proposed OTA-FL-ISCC schemes significantly outperforms those without ISCC design. Consequently, the OTA-FL-ISCC scheme achieves faster convergence with reduced energy consumption and latency. Moreover, Fig. 9 compares the weighted sum of training latency and energy consumption over different schemes under various weight factors  $w$ . Comparing with OTA-FL, the OTA-FL-FCR achieves a lower weighted sum of training latency and energy consumption due to computation resource optimization. Meanwhile, significant reductions in latency and

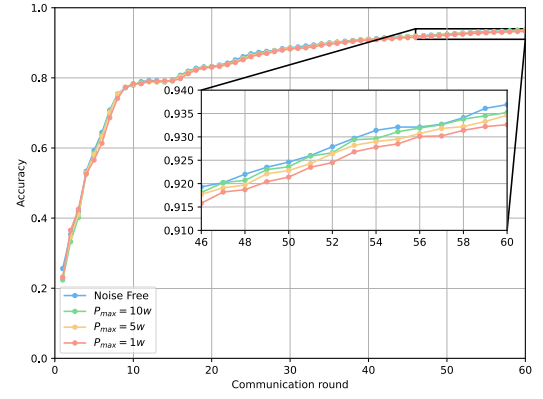


Fig. 11. Performance evaluation over various power allocation strategies.

energy are achieved by optimizing the sample sensing strategy. Therefore, the proposed OTA-FL-ISCC scheme achieves the lowest weighted sum of network latency and energy consumption among all schemes.

In Fig. 10, we also provide the training latency and energy consumption of each communication round over different collection strategies with learning performance (24e) satisfied. It is shown that both the training latency and energy of OTA-FL-ISCC with PSC strategy are the lowest compared to OTA-FL and OTA-FL-ISCC with DSC strategy. In specific, the OTA-FL always maintains high latency and energy, while OTA-FL-ISCC's latency and energy increase with the number of communication rounds due to the accumulation of dataset, which demonstrate the effectiveness of the proposed OTA-FL-ISCC. Fig. 11 presents the test accuracy under various power allocation. Here, the *Noise free* serves as a benchmark, indicating perfect aggregation without any errors in the communication process. From Fig. 11, it is shown that the proposed power allocation strategy achieves similar convergence to the *Noise free* strategy. Furthermore, it is observed that the performance under  $p_{\max} = 10$  W generally outperforms that of  $p_{\max} = 1$  W. This suggests that a larger power budget has greater capability to mitigate the impact of channel noise.

#### D. Practical Consideration of the Proposed Framework

In this subsection, we deploy our proposed framework under a more practical environment, which typically encounters various challenges, such as unreliable network connections, device malfunctions, heterogeneous device capabilities, irregular data distributions, and adversarial attacks.

Under the unreliable networks, heterogeneous device capabilities, and device malfunctions environment that result in device dropouts, we evaluate the framework accuracy with varying numbers of participating devices, as illustrated in Fig. 12. To simulate device dropout, we randomly disconnect devices during each round of model aggregation. It demonstrates that the proposed framework achieves a comparable convergence performance with the decrement of gradient aggregation participating devices, which indicates its robustness to dropout issues.

For irregular data distributions leading to Non-IID datasets, we evaluate the convergence of our proposed framework under

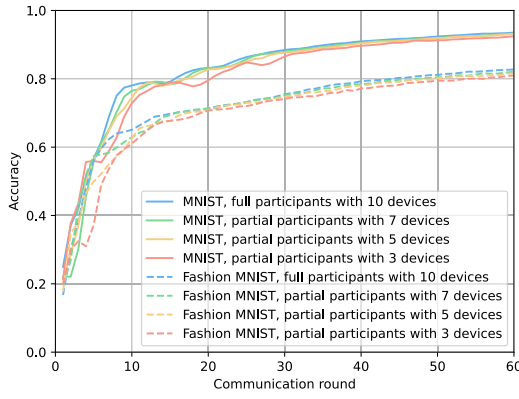


Fig. 12. Performance evaluation under potential dropout issues.

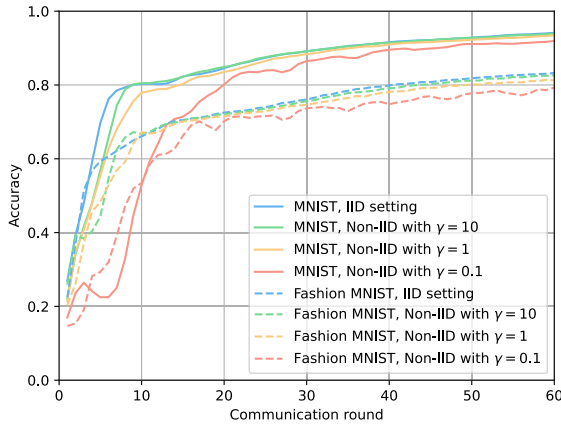


Fig. 13. Performance evaluation under Non-IID datasets.

varying degrees of Non-IID settings, as shown in Fig. 13. The Dirichlet distribution is used to model label distribution skew among devices, with the parameter  $\gamma$  representing the degree of Non-IID datasets. Here, a lower  $\gamma$  value corresponds to a more skewed Non-IID dataset. As depicted in Fig. 13, the convergence performance decreases with the decrement of  $\gamma$ , however it wouldn't generate a large gap even with extremely small value of  $\gamma$ . It suggests that the proposed framework can avoid the performance degradation effectively caused by irregular data distributions, which demonstrates its resilience to Non-IID datasets.

In terms of the security issue, Fig. 14 illustrates the training accuracy under data poisoning attacks with various malicious devices and poisoning rates. From this figure, we can find that the training accuracy keeps unchanged under varying poisoning rates under the same number of malicious devices. On the other hand, the training accuracy decreases with the increment of malicious devices.

Regarding to the privacy issue, Fig. 15 illustrates the reconstructed images under inversion attacks with the data reconstruction method [41]. It demonstrates that the proposed mechanism can effectively protect data privacy compared with the existing FedSGD mechanism [3]. Furthermore, existing methods, such as secure multi-party computation and homomorphic encryption, can also be integrated into our framework to further protect the data privacy.

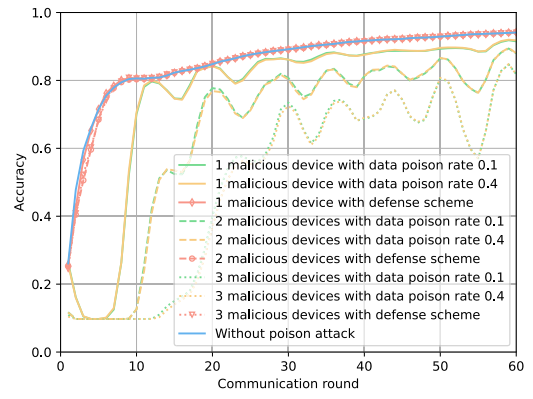


Fig. 14. Performance evaluation under data poisoning attacks.

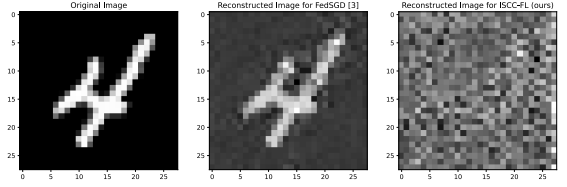


Fig. 15. Performance evaluation under inversion attacks.

## VI. CONCLUSION

This work considered an OTA-FL-ISCC scheme to achieve communication-and-energy efficient FL, where sensing, communication and computation are jointly considered throughout the FL procedure. Specifically, we first derived an ATE metric to characterized learning performance of proposed framework by convergence analyses. Then, we investigated a training latency and energy consumption minimization problem with ATE guarantees. Furthermore, a joint sensing, communication and computation resource allocation strategy was developed, where a DRL algorithm that nests convex optimization with DQN was designed. Numerical results verified our convergence analyses, and demonstrated the effectiveness of our developed resource management algorithm.

### APPENDIX A PROOF OF LEMMA 1

According to the definition of local loss function in (1), we have the following translation of

$$\begin{aligned}
 F(\mathbf{w}_{t-1}^n; \mathcal{S}_t^n) &= \frac{1}{S_t^n} \left[ \sum_{(\mathbf{x}_j, y_j) \in \mathcal{S}_{t-1}^n} f(\mathbf{w}_{t-1}^n, (\mathbf{x}_j, y_j)) \right. \\
 &\quad \left. + \sum_{(\mathbf{x}_j, y_j) \in \mathcal{D}_t^n} f(\mathbf{w}_{t-1}^n, (\mathbf{x}_j, y_j)) \right] \\
 &= \frac{S_{t-1}^n}{S_t^n} F(\mathbf{w}_{t-1}^n; \mathcal{S}_{t-1}^n) + \frac{D_t^n}{S_t^n} F(\mathbf{w}_{t-1}^n; \mathcal{D}_t^n).
 \end{aligned} \tag{44}$$

Thus, the global loss function can be further rewritten as

$$\begin{aligned}
 F(\mathbf{w}_{t-1}; \mathcal{S}_t) &= \frac{1}{S_t} \sum_{n=0}^{N-1} \left( \frac{S_{t-1}^n F(\mathbf{w}_{t-1}^n; \mathcal{S}_{t-1}^n)}{S_{t-1}} S_{t-1} \right)
 \end{aligned}$$



$$\begin{aligned}
& + \frac{D_t^n F(\mathbf{w}_{t-1}^n; \mathcal{D}_t^n)}{D_t} D_t \Big) \\
& = \frac{S_{t-1}}{S_t} F(\mathbf{w}_{t-1}; \mathcal{S}_{t-1}) + \frac{D_t}{S_t} F(\mathbf{w}_{t-1}; \mathcal{D}_t). \quad (45)
\end{aligned}$$

Taking derivative of the the global loss function  $F$  with respect to  $\mathbf{w}_{t-1}$  over both sides of (45), Lemma 1 can be obtained. This ends the proof.

## APPENDIX B PROOF OF LEMMA 2

To proof Lemma 2, we first derive the improvement at the first communication round, and then extended to the rest communication rounds.

### A. Improvement in the First Communication Round

The AI model is updated based on initialization  $\mathbf{w}_0$  over the new sensed dataset  $\mathcal{D}_1$  in the current round. According to the assumption of **L-smoothness**, the improvement on the global loss can be expressed as:

$$\begin{aligned}
& F(\mathbf{w}_1; \mathcal{S}_1) - F(\mathbf{w}_0; \mathcal{S}_0) \\
& \leq \langle \nabla F(\mathbf{w}_0; \mathcal{D}_1), \mathbf{w}_1 - \mathbf{w}_0 \rangle + \frac{L}{2} \|\mathbf{w}_1 - \mathbf{w}_0\|^2 \\
& = \eta \underbrace{\langle \nabla F(\mathbf{w}_0; \mathcal{D}_1), \boldsymbol{\varepsilon}_1 - \nabla F(\mathbf{w}_0; \mathcal{D}_1) \rangle}_{A_1} \\
& \quad + \frac{L\eta^2}{2} \underbrace{\|-\nabla F(\mathbf{w}_0; \mathcal{D}_1) + \boldsymbol{\varepsilon}_1\|^2}_{B_1}. \quad (46)
\end{aligned}$$

Now we aim to find the upper bound for  $A_1$  and  $B_1$ , respectively. Specifically, for  $A_1$ , we have

$$\begin{aligned}
A_1 & = \langle \nabla F(\mathbf{w}_0; \mathcal{D}_1), -\nabla F(\mathbf{w}_0; \mathcal{D}_1) \rangle + \langle \nabla F(\mathbf{w}_0; \mathcal{D}_1), \boldsymbol{\varepsilon}_1 \rangle \\
& \stackrel{(c)}{\leq} -\|\nabla F(\mathbf{w}_0; \mathcal{D}_1)\|^2 + \frac{\|\nabla F(\mathbf{w}_0; \mathcal{D}_1)\|^2}{2} + \frac{\|\boldsymbol{\varepsilon}_1\|^2}{2} \\
& = -\frac{\|\nabla F(\mathbf{w}_0; \mathcal{D}_1)\|^2}{2} + \frac{\|\boldsymbol{\varepsilon}_1\|^2}{2}, \quad (47)
\end{aligned}$$

where (c) comes from the arithmetic mean-geometric mean (AM-GM) inequality. Similarly,  $B_1$  is bounded by

$$\begin{aligned}
B_1 & = \|\nabla F(\mathbf{w}_0; \mathcal{D}_1)\|^2 + \|\boldsymbol{\varepsilon}_1\|^2 - 2 \langle \nabla F(\mathbf{w}_0; \mathcal{D}_1), \boldsymbol{\varepsilon}_1 \rangle \\
& \leq 2 \|\nabla F(\mathbf{w}_0; \mathcal{D}_1)\|^2 + 2 \|\boldsymbol{\varepsilon}_1\|^2. \quad (48)
\end{aligned}$$

Taking the expectation at both sides of (46), we have

$$\begin{aligned}
& \mathbb{E}(F(\mathbf{w}_1; \mathcal{S}_1) - F(\mathbf{w}_0; \mathcal{S}_0)) \\
& \leq -\eta \left( \frac{1}{2} - L\eta \right) \mathbb{E}(\|\nabla F(\mathbf{w}_0; \mathcal{D}_1)\|^2) \\
& \quad + \eta \left( L\eta + \frac{1}{2} \right) \mathbb{E}(\|\boldsymbol{\varepsilon}_1\|^2) \\
& \stackrel{(d)}{\leq} -\frac{\eta}{2} \mathbb{E}(\|\nabla F(\mathbf{w}_0; \mathcal{S}_0)\|^2) + L\eta^2 G_1 \\
& \quad + \eta \left( L\eta + \frac{1}{2} \right) \mathbb{E}(\|\boldsymbol{\varepsilon}_1\|^2) \\
& \stackrel{(e)}{\leq} -\frac{\eta}{2} \mathbb{E}(\|\nabla F(\mathbf{w}_0; \mathcal{S}_0)\|^2) + \eta G_1 + \frac{3\eta}{2} \mathbb{E}(\|\boldsymbol{\varepsilon}_1\|^2), \quad (49)
\end{aligned}$$

where (d) is derived from Assumption 2, and (e) is achieved by letting  $\eta \leq \frac{1}{L}$ .

2) *Improvement in the rest communication rounds:* For the rest communication rounds, the AI model is updated based on both the accumulative dataset  $\mathcal{S}_{t-1}$  and the newly sensed dataset  $\mathcal{D}_t$ . Recall (14) in Assumption 1, it follows that

$$\begin{aligned}
& F(\mathbf{w}_t; \mathcal{S}_t) - F(\mathbf{w}_{t-1}; \mathcal{S}_{t-1}) \\
& \leq \langle \nabla F(\mathbf{w}_{t-1}; \mathcal{S}_{t-1}), \mathbf{w}_t - \mathbf{w}_{t-1} \rangle \\
& \quad + \frac{L}{2} \|\mathbf{w}_t - \mathbf{w}_{t-1}\|^2 \\
& = \eta \underbrace{\langle \nabla F(\mathbf{w}_{t-1}; \mathcal{S}_{t-1}), -\nabla F(\mathbf{w}_{t-1}; \mathcal{S}_t) + \boldsymbol{\varepsilon}_t \rangle}_{A_2} \\
& \quad + \frac{L\eta^2}{2} \underbrace{\|-\nabla F(\mathbf{w}_{t-1}; \mathcal{S}_t) + \boldsymbol{\varepsilon}_t\|^2}_{B_2}. \quad (50)
\end{aligned}$$

Based on Lemma 1,  $A_2$  in (50) can be rearranged as

$$\begin{aligned}
A_2 & = \left\langle \nabla F(\mathbf{w}_{t-1}; \mathcal{S}_{t-1}), -\frac{S_{t-1}}{S_t} \nabla F(\mathbf{w}_{t-1}; \mathcal{S}_{t-1}) \right. \\
& \quad \left. - \frac{D_t}{S_t} \nabla F(\mathbf{w}_{t-1}; \mathcal{D}_t) + \boldsymbol{\varepsilon}_t \right\rangle \\
& = -\frac{S_{t-1}}{S_t} \|\nabla F(\mathbf{w}_{t-1}; \mathcal{S}_{t-1})\|^2 + \langle \nabla F(\mathbf{w}_{t-1}; \mathcal{S}_{t-1}), \boldsymbol{\varepsilon}_t \rangle \\
& \quad - \frac{D_t}{S_t} \langle \nabla F(\mathbf{w}_{t-1}; \mathcal{S}_{t-1}), \nabla F(\mathbf{w}_{t-1}; \mathcal{D}_t) \rangle. \quad (51)
\end{aligned}$$

Similarly,  $B_2$  in (50) can be expressed as

$$\begin{aligned}
B_2 & = \|\nabla F(\mathbf{w}_{t-1}; \mathcal{S}_t)\|^2 + \|\boldsymbol{\varepsilon}_t\|^2 - 2 \langle \nabla F(\mathbf{w}_{t-1}; \mathcal{S}_t), \boldsymbol{\varepsilon}_t \rangle \\
& = \left( \frac{S_{t-1}}{S_t} \right)^2 \|\nabla F(\mathbf{w}_{t-1}; \mathcal{S}_{t-1})\|^2 \\
& \quad + \left( \frac{D_t}{S_t} \right)^2 \|\nabla F(\mathbf{w}_{t-1}; \mathcal{D}_t)\|^2 \\
& \quad + 2 \frac{S_{t-1} D_t}{(S_t)^2} \langle \nabla F(\mathbf{w}_{t-1}; \mathcal{S}_{t-1}), \nabla F(\mathbf{w}_{t-1}; \mathcal{D}_t) \rangle + \|\boldsymbol{\varepsilon}_t\|^2 \\
& \quad - 2 \frac{D_t}{S_t} \langle \nabla F(\mathbf{w}_{t-1}; \mathcal{D}_t), \boldsymbol{\varepsilon}_t \rangle \\
& \quad - 2 \frac{S_{t-1}}{S_t} \langle \nabla F(\mathbf{w}_{t-1}; \mathcal{S}_{t-1}), \boldsymbol{\varepsilon}_t \rangle. \quad (52)
\end{aligned}$$

As a result, we have

$$\begin{aligned}
& F(\mathbf{w}_t; \mathcal{S}_t) - F(\mathbf{w}_{t-1}; \mathcal{S}_{t-1}) \\
& \leq \frac{L\eta^2}{2} \left( \frac{D_t}{S_t} \right)^2 \|\nabla F(\mathbf{w}_{t-1}; \mathcal{D}_t)\|^2 \\
& \quad + \left[ \frac{L\eta^2}{2} \left( \frac{S_{t-1}}{S_t} \right)^2 - \eta \frac{S_{t-1}}{S_t} \right] \|\nabla F(\mathbf{w}_{t-1}; \mathcal{S}_{t-1})\|^2 \\
& \quad + \frac{L\eta^2}{2} \|\boldsymbol{\varepsilon}_t\|^2 \\
& \quad - \underbrace{\eta \frac{D_t}{S_t} \left( 1 - L\eta \frac{S_{t-1}}{S_t} \right) \langle \nabla F(\mathbf{w}_{t-1}; \mathcal{S}_{t-1}), \nabla F(\mathbf{w}_{t-1}; \mathcal{D}_t) \rangle}_C \\
& \quad + \underbrace{\eta \left( 1 - L\eta \frac{S_{t-1}}{S_t} \right) \langle \nabla F(\mathbf{w}_{t-1}; \mathcal{S}_{t-1}), \boldsymbol{\varepsilon}_t \rangle}_D
\end{aligned}$$

$$\underbrace{-L\eta^2 \frac{D_t}{S_t} \langle \nabla F(\mathbf{w}_{t-1}; \mathcal{D}_t), \boldsymbol{\varepsilon}_t \rangle}_E. \quad (53)$$

Now, we aim to find the upper bounds of  $C$ ,  $D$ , and  $E$  in (53). Let  $1 - L\eta \frac{S_{t-1}}{S_t} \geq 0$  and apply the AM-GM inequality, we have

$$C \leq \eta \frac{D_t}{S_t} \left(1 - L\eta \frac{S_{t-1}}{S_t}\right) \left[ \frac{\|\nabla F(\mathbf{w}_{t-1}; \mathcal{S}_{t-1})\|^2}{2} + \frac{\|\nabla F(\mathbf{w}_{t-1}; \mathcal{D}_t)\|^2}{2} \right], \quad (54)$$

and

$$D \leq \eta \left(1 - L\eta \frac{S_{t-1}}{S_t}\right) \left[ \frac{\|\nabla F(\mathbf{w}_{t-1}; \mathcal{S}_{t-1})\|^2}{2} + \frac{\|\boldsymbol{\varepsilon}_t\|^2}{2} \right]. \quad (55)$$

By applying the Cauchy-Schwarz and AM-GM inequalities, we have

$$E \leq L\eta^2 \frac{D_t}{S_t} \left[ \frac{\|\nabla F(\mathbf{w}_{t-1}; \mathcal{D}_t)\|^2}{2} + \frac{\|\boldsymbol{\varepsilon}_t\|^2}{2} \right] \quad (56)$$

By taking the expectation at both sides of (50), (53) can be further bounded by

$$\begin{aligned} & \mathbb{E}(F(\mathbf{w}_t; \mathcal{S}_t) - F(\mathbf{w}_{t-1}; \mathcal{S}_{t-1})) \\ & \leq \left[ \frac{L\eta^2}{2} \left(1 - \frac{S_{t-1}}{S_t} + \frac{D_t}{S_{t-1}}\right) \right. \\ & \quad + \frac{\eta}{2} \mathbb{E}(\|\boldsymbol{\varepsilon}_t\|^2) + \left[ \frac{L\eta^2 D_t}{2 S_t} \left(\frac{D_t}{S_t} - \frac{S_{t-1}}{S_t} + 1\right) \right. \\ & \quad + \frac{\eta}{2} \left(\frac{D_t}{S_t}\right) \mathbb{E}(\|\nabla F(\mathbf{w}_{t-1}; \mathcal{D}_t)\|^2) \\ & \quad + \left[ \frac{\eta}{2} \left(1 - \frac{2S_{t-1}}{S_t} + \frac{D_t}{S_t}\right) \right. \\ & \quad + \left. \left. \frac{L\eta^2 S_{t-1}}{2 S_t} \left(\frac{S_{t-1}}{S_t} - \frac{D_t}{S_t} - 1\right)\right] \mathbb{E}(\|\nabla F(\mathbf{w}_{t-1}; \mathcal{S}_{t-1})\|^2) \right] \\ & \stackrel{(f)}{\leq} -\frac{\eta S_{t-1}}{2 S_t} \mathbb{E}(\|\nabla F(\mathbf{w}_{t-1}; \mathcal{S}_{t-1})\|^2) \\ & \quad + \frac{\eta}{2} \left(1 + \frac{2D_t}{S_{t-1}}\right) \mathbb{E}(\|\boldsymbol{\varepsilon}_t\|^2) \\ & \quad + \left[ \frac{\eta D_t}{2 S_{t-1}} \left(\frac{D_t}{S_t} + 1\right) \right] \mathbb{E}\|\nabla F(\mathbf{w}_{t-1}; \mathcal{D}_t)\|^2 \\ & \stackrel{(g)}{\leq} -\frac{\eta}{2} \mathbb{E}(\|\nabla F(\mathbf{w}_{t-1}; \mathcal{S}_{t-1})\|^2) + \underbrace{\left(\frac{2D_t}{S_{t-1}}\right) \frac{G_t \eta}{2}}_{\text{sensing related effect}} \\ & \quad + \underbrace{\frac{\eta}{2} \left(1 + \frac{2D_t}{S_{t-1}}\right) \mathbb{E}(\|\boldsymbol{\varepsilon}_t\|^2)}_{\text{sensing \& communication related effect}}, \quad (57) \end{aligned}$$

where (f) comes from  $\eta \leq \frac{1}{L} \frac{S_t}{S_{t-1}}$ , and (g) comes from Assumption 2. This ends the proof.

## REFERENCES

- [1] T. Li, A. K. Sahu, A. Talwalkar, and V. Smith, "Federated learning: Challenges, methods, and future directions," *IEEE Signal Process. Mag.*, vol. 37, no. 3, pp. 50–60, May 2020.
- [2] K. B. Letaief, Y. Shi, J. Lu, and J. Lu, "Edge artificial intelligence for 6G: Vision, enabling technologies, and applications," *IEEE J. Sel. Areas Commun.*, vol. 40, no. 1, pp. 5–36, Jan. 2022.
- [3] B. McMahan, E. Moore, D. Ramage, S. Hampson, and B. A. Y. Arcas, "Communication-efficient learning of deep networks from decentralized data," in *Proc. Int. Conf. Artif. Intell. Statist. (AISTATS)*, Lauderdale, FL, USA, 2017, pp. 1273–1282.
- [4] K. B. Letaief, W. Chen, Y. Shi, J. Zhang, and Y. A. Zhang, "The roadmap to 6G: AI empowered wireless networks," *IEEE Commun. Mag.*, vol. 57, no. 8, pp. 84–90, Aug. 2019.
- [5] W. Saad, M. Bennis, and M. Chen, "A vision of 6G wireless systems: Applications, trends, technologies, and open research problems," *IEEE Netw.*, vol. 34, no. 3, pp. 134–142, May/Jun. 2020.
- [6] Y. Shi, K. Yang, T. Jiang, J. Zhang, and K. B. Letaief, "Communication-efficient edge AI: Algorithms and systems," *IEEE Commun. Surveys Tuts.*, vol. 22, no. 4, pp. 2167–2191, 4th Quart., 2020.
- [7] K. Cheng, F. Guo, and M. Peng, "An efficient distributed machine learning framework in wireless D2D networks: Convergence analysis and system implementation," *IEEE Trans. Veh. Technol.*, vol. 72, no. 5, pp. 6723–6738, May 2023.
- [8] G. Zhu, Y. Du, D. Gunduz, and K. Huang, "One-bit over-the-air aggregation for communication-efficient federated edge learning: Design and convergence analysis," *IEEE Trans. Wireless Commun.*, vol. 20, no. 3, pp. 2120–2135, Mar. 2021.
- [9] Y. Sun, S. Zhou, Z. Niu, and D. Gündüz, "Dynamic scheduling for over-the-air federated edge learning with energy constraints," *IEEE J. Sel. Areas Commun.*, vol. 40, no. 1, pp. 227–242, Jan. 2022.
- [10] M. Chen, Z. Yang, W. Saad, C. Yin, H. V. Poor, and S. Cui, "A joint learning and communications framework for federated learning over wireless networks," *IEEE Trans. Wireless Commun.*, vol. 20, no. 1, pp. 269–283, Jan. 2021.
- [11] S. Wang et al., "Adaptive federated learning in resource constrained edge computing systems," *IEEE J. Sel. Areas Commun.*, vol. 37, no. 6, pp. 1205–1221, Jun. 2019.
- [12] P. Liu et al., "Toward ambient intelligence: Federated edge learning with task-oriented sensing, computation, and communication integration," *IEEE J. Sel. Topics Signal Process.*, vol. 17, no. 1, pp. 158–172, Jan. 2023.
- [13] P. Liu, G. Zhu, W. Jiang, W. Luo, J. Xu, and S. Cui, "Vertical federated edge learning with distributed integrated sensing and communication," *IEEE Wireless Commun. Lett.*, vol. 26, no. 9, pp. 2091–2095, Sep. 2022.
- [14] P. Zhang et al., "Toward intelligent and efficient 6G networks: JCSC enabled on-purpose machine communications," *IEEE Wireless Commun.*, vol. 30, no. 1, pp. 150–157, Feb. 2023.
- [15] Z. Feng, Z. Wei, X. Chen, H. Yang, Q. Zhang, and P. Zhang, "Joint communication, sensing, and computation enabled 6G intelligent machine system," *IEEE Netw.*, vol. 35, no. 6, pp. 34–42, Nov./Dec. 2021.
- [16] G. Zhu et al., "Pushing AI to wireless network edge: An overview on integrated sensing, communication, and computation towards 6G," *Sci. China Inf. Sci.*, vol. 66, no. 3, Mar. 2023, Art. no. 130301.
- [17] D. Wen et al., "Task-oriented sensing, computation, and communication integration for multi-device edge AI," *IEEE Trans. Wireless Commun.*, vol. 23, no. 3, pp. 2486–2502, Mar. 2024.
- [18] Q. Qi, X. Chen, A. Khalili, C. Zhong, Z. Zhang, and D. W. K. Ng, "Integrating sensing, computing, and communication in 6G wireless networks: Design and optimization," *IEEE Trans. Commun.*, vol. 70, no. 9, pp. 6212–6227, Sep. 2022.
- [19] Z. Yang, M. Chen, W. Saad, C. S. Hong, and M. Shikh-Bahaei, "Energy efficient federated learning over wireless communication networks," *IEEE Trans. Wireless Commun.*, vol. 20, no. 3, pp. 1935–1949, Mar. 2021.
- [20] X. Mo and J. Xu, "Energy-efficient federated edge learning with joint communication and computation design," *J. Commun. Inf. Netw.*, vol. 6, no. 2, pp. 110–124, Jun. 2021.
- [21] M. S. Al-Abiad, M. Z. Hassan, and M. J. Hossain, "Energy-efficient resource allocation for federated learning in NOMA-enabled and relay-assisted Internet of Things networks," *IEEE Internet Things J.*, vol. 9, no. 24, pp. 24736–24753, Dec. 2022.

- [22] Q. Chen, X. Xu, Z. You, H. Jiang, J. Zhang, and F.-Y. Wang, "Communication-efficient federated edge learning for NR-U-based IIoT networks," *IEEE Internet Things J.*, vol. 9, no. 14, pp. 12450–12459, Jul. 2022.
- [23] M. Chen, N. Shlezinger, H. V. Poor, Y. C. Eldar, and S. Cui, "Joint resource management and model compression for wireless federated learning," in *Proc. IEEE Int. Conf. Commun.*, Montreal, QC, Canada, Jun. 2021, pp. 1–6.
- [24] G. Zhu, Y. Wang, and K. Huang, "Broadband analog aggregation for low-latency federated edge learning," *IEEE Trans. Wireless Commun.*, vol. 19, no. 1, pp. 491–506, Jan. 2020.
- [25] Y. Shao, D. Gunduz, and S. C. Liew, "Federated edge learning with misaligned over-the-air computation," *IEEE Trans. Wireless Commun.*, vol. 21, no. 6, pp. 3951–3964, Jun. 2022.
- [26] K. Yang, T. Jiang, Y. Shi, and Z. Ding, "Federated learning via over-the-air computation," *IEEE Trans. Wireless Commun.*, vol. 19, no. 3, pp. 2022–2035, Mar. 2020.
- [27] M. M. Amiri and D. Gündüz, "Machine learning at the wireless edge: Distributed stochastic gradient descent over-the-air," *IEEE Trans. Signal Process.*, vol. 68, pp. 2155–2169, 2020.
- [28] A. Elgabli, J. Park, C. B. Issaid, and M. Bennis, "Harnessing wireless channels for scalable and privacy-preserving federated learning," *IEEE Trans. Commun.*, vol. 69, no. 8, pp. 5194–5208, Aug. 2021.
- [29] N. Zhang and M. Tao, "Gradient statistics aware power control for over-the-air federated learning," *IEEE Trans. Wireless Commun.*, vol. 20, no. 8, pp. 5115–5128, Aug. 2021.
- [30] X. Cao, G. Zhu, J. Xu, and S. Cui, "Transmission power control for over-the-air federated averaging at network edge," *IEEE J. Sel. Areas Commun.*, vol. 40, no. 5, pp. 1571–1586, May 2022.
- [31] T. Gafni, K. Cohen, and Y. C. Eldar, "Federated learning from heterogeneous data via controlled Bayesian air aggregation," 2023, *arXiv:2303.17413*.
- [32] T. Sery, N. Shlezinger, K. Cohen, and Y. C. Eldar, "Over-the-air federated learning from heterogeneous data," *IEEE Trans. Signal Process.*, vol. 69, pp. 3796–3811, 2021.
- [33] L. Li et al., "Energy and spectrum efficient federated learning via high-precision over-the-air computation," *IEEE Trans. Wireless Commun.*, vol. 23, no. 2, pp. 1228–1242, Feb. 2024.
- [34] Y. Liang, Q. Chen, G. Zhu, and H. Jiang, "Theoretical analysis and performance evaluation for federated edge learning with integrated sensing, communication and computation," in *Proc. IEEE Int. Conf. Commun. Workshops (ICC Workshops)*, Rome, Italy, May 2023, pp. 592–598.
- [35] S. Wang, Y.-C. Wu, M. Xia, R. Wang, and H. V. Poor, "Machine intelligence at the edge with learning centric power allocation," *IEEE Trans. Wireless Commun.*, vol. 19, no. 11, pp. 7293–7308, Nov. 2020.
- [36] T. Zhang, S. Wang, G. Li, F. Liu, G. Zhu, and R. Wang, "Accelerating edge intelligence via integrated sensing and communication," in *Proc. IEEE Int. Conf. Commun.*, May 2022, pp. 1586–1592.
- [37] A. Ghosh et al., *Fundamentals of LTE*. Upper Saddle River, NJ, USA: Prentice-Hall, 2010.
- [38] R. S. Sutton and A. G. Barto, *Introduction To Reinforcement Learning*, 1st ed., Cambridge, MA, USA: MIT Press, 1998.
- [39] W. Liu, X. Zang, Y. Li, and B. Vucetic, "Over-the-air computation systems: Optimization, analysis and scaling laws," *IEEE Trans. Wireless Commun.*, vol. 19, no. 8, pp. 5488–5502, Aug. 2020.
- [40] W. Zhang et al., "Optimizing federated learning in distributed industrial IoT: A multi-agent approach," *IEEE J. Sel. Areas Commun.*, vol. 39, no. 12, pp. 3688–3703, Dec. 2021.
- [41] L. Zhu, Z. Liu, and S. Han, "Deep leakage from gradients," in *Proc. Int. Conf. Neural Inf. Process. Syst.*, Vancouver, BC, Canada, 2018, pp. 14774–14784.



**Yipeng Liang** (Graduate Student Member, IEEE) is currently pursuing the Ph.D. degree with the Electronic Information School, Wuhan University, Wuhan, China. His research interests include wireless networks, edge AI, federated learning, and resource management.



**Qimei Chen** (Member, IEEE) received the Ph.D. degree from the College of Information Science and Electronic Engineering, Zhejiang University, Hangzhou, China, in 2017. She was a Visiting Student with the Department of Electrical and Computer Engineering, University of California at Davis, Davis, CA, USA, from 2015 to 2016. From 2017 to 2022, she was an Associate Researcher with the School of Electric Information, Wuhan University, Wuhan, China, where she has been an Associate Professor, since 2023. Her research interests include intelligent edge communication, unlicensed spectrum, massive MIMO-NOMA, and machine learning in wireless communications. She received the Exemplary Reviewer Certificate of IEEE WIRELESS COMMUNICATIONS LETTERS in 2020 and 2023. She has served as the Workshop Co-Chair and a TPC Member for IEEE conferences, such as ICC, GLOBECOM, PIMRC, and WCNC. She also served as a Guest Editor for the Special Issues on Heterogeneous Networks of Sensors and NOMA in ISAC (MDPI).



**Guangxu Zhu** (Member, IEEE) received the Ph.D. degree in electrical and electronic engineering from The University of Hong Kong in 2019. Currently, he is a Senior Research Scientist and the Deputy Director of the Network System Optimization Center, Shenzhen Research Institute of Big Data; and an Adjunct Associate Professor with The Chinese University of Hong Kong, Shenzhen. His current research interests include edge intelligence, semantic communications, and integrated sensing and communication. He was a recipient of the 2023 IEEE ComSoc Asia-Pacific Best Young Researcher Award and the Outstanding Paper Award, the World's Top 2% Scientists by Stanford University, the 2022 AI 2000 Most Influential Scholar Award Honorable Mention, the Young Scientist Award from UCOM 2023, and the Best Paper Award from WCSP 2013 and IEEE JSnC 2024. He serves as the Track/Symposium/Workshop Co-Chair for several IEEE major conferences, including IEEE PIMRC 2021, WCSP 2023, IEEE Globecom 2023, VTC-fall 2023, ICASSP 2024, and WCNC 2024. He is the Vice Co-Chair of the IEEE ComSoc Asia-Pacific Board Young Professionals Committee. He serves as an Associate Editor for top-tier journal in ComSoc, including IEEE TRANSACTIONS ON WIRELESS COMMUNICATIONS and IEEE WIRELESS COMMUNICATIONS LETTERS.



**Hao Jiang** (Member, IEEE) received the B.Eng. degree in communication engineering and the M.Eng. and Ph.D. degrees in communication and information systems from Wuhan University, Wuhan, China, in 1999, 2001, and 2004, respectively. He was a Post-Doctoral Research Fellow with LIMOS, Clermont-Ferrand, France, from 2004 to 2005; and a Visiting Professor with the University of Calgary, Calgary, AB, Canada, and ISIMA, Blaise Pascal University, Clermont-Ferrand. He is currently a Professor with Wuhan University. He has authored over 60 papers in different journals and conferences. His research interests include mobile ad hoc networks and mobile big data.



**Yonina C. Eldar** (Fellow, IEEE) received the B.Sc. degree in physics and the another B.Sc. degree in electrical engineering from Tel-Aviv University and the Ph.D. degree in electrical engineering and computer science from MIT in 2002. She is a Professor with the Department of Mathematics and Computer Science, Weizmann Institute of Science, Rehovot, Israel, where she heads the Center for Biomedical Engineering and Signal Processing and holds the Dorothy and Patrick Gorman Professorial Chair. She is also a Visiting Professor with MIT, a Visiting Sci-

entist with the Broad Institute, and an Adjunct Professor with Duke University. She was a Visiting Professor with Stanford University. She is a member of Israel Academy of Sciences and Humanities and a EURASIP Fellow. She was a Horev Fellow of the Leaders in Science and Technology Program, Technion; and an Alon Fellow. She has received many awards for excellence in research and teaching, including the IEEE Signal Processing Society Technical Achievement Award in 2013, the IEEE/AESS Fred Nathanson Memorial Radar Award in 2014, and the IEEE Kiyo Tomiyasu Award in 2016. She also received the Michael Bruno Memorial Award from the Rothschild Foundation, the Weizmann Prize for Exact Sciences, the Wolf Foundation Krill Prize for Excellence in Scientific Research, the Henry Taub Prize for Excellence in Research (twice), the Hershel Rich Innovation Award (three times), and the Award for Women with Distinguished Contributions. She received several best paper awards and best demo awards together with her research students and colleagues. She was selected as one of the 50 most influential women in Israel and a member of the Israel Committee for Higher Education. She is a member of several IEEE technical committees and award committees, and heads the Committee for Promoting Gender Fairness in Higher Education Institutions in Israel. She is the Editor-in-Chief of *Foundations and Trends in Signal Processing*.



**Shuguang Cui** (Fellow, IEEE) received the Ph.D. degree in electrical engineering from Stanford University, California, USA, in 2005. Afterwards, he was an Assistant Professor, an Associate Professor, a Full Professor, and the Chair Professor in electrical and computer engineering with The University of Arizona, Texas A&M University, UC Davis, and The Chinese University of Hong Kong at Shenzhen, respectively. He was also the Executive Dean of the School of Science and Engineering, The Chinese University of Hong Kong, Shenzhen, China; the

Executive Vice Director of Shenzhen Research Institute of Big Data; and the Director of Shenzhen Future Network of Intelligence Institute (FNii-Shenzhen), Shenzhen. His current research interests focus on the merging between AI and communication networks. He was a fellow of both Canadian Academy of Engineering and the Royal Society of Canada. He was a recipient of the IEEE Signal Processing Society 2012 Best Paper Award. In 2020, he won the IEEE ICC Best Paper Award, the ICIP Best Paper Finalist, and the IEEE Globecom Best Paper Award. In 2021, he won the IEEE WCNC Best Paper Award. In 2023, he won the IEEE Marconi Best Paper Award. He has served as the general co-chair and the TPC co-chair for many IEEE conferences. He has been an Elected Member of IEEE Signal Processing Society SPCOM Technical Committee (2009–2014) and the Elected Chair of IEEE ComSoc Wireless Technical Committee (2017–2018). He is a member of the Steering Committee for IEEE TRANSACTIONS ON BIG DATA and the Chair of the Steering Committee for IEEE TRANSACTIONS ON COGNITIVE COMMUNICATIONS AND NETWORKING. He is also the Vice Chair of the IEEE VT Fellow Evaluation Committee and a member of the IEEE ComSoc Award Committee. He was selected as the Thomson Reuters Highly Cited Researcher and listed in the Worlds' Most Influential Scientific Minds by ScienceWatch in 2014. He has been serving as an Area Editor for *IEEE Signal Processing Magazine*; and an Associate Editor for IEEE TRANSACTIONS ON BIG DATA, IEEE TRANSACTIONS ON SIGNAL PROCESSING, IEEE JOURNAL ON SELECTED AREAS IN COMMUNICATIONS Series on Green Communications and Networking, and IEEE TRANSACTIONS ON WIRELESS COMMUNICATIONS. In 2023, he starts to serve as the Editor-in-Chief for IEEE TRANSACTIONS ON MOBILE COMPUTING. He was elected as an IEEE ComSoc Distinguished Lecturer in 2014 and an IEEE VT Society Distinguished Lecturer in 2019.